Pch2 orchestrates the meiotic recombination checkpoint from the cytoplasm

Esther Herruzo[1], Ana Lago-Maciel[1], Sara Baztán[1], Beatriz Santos[1,2], Jesús A. Carballo[3] and Pedro A. San-Segundo[1,*]

[1]Instituto de Biología Funcional y Genómica (IBFG). Consejo Superior de Investigaciones Científicas (CSIC) and University of Salamanca. 37007-Salamanca, Spain

[2]Departamento de Microbiología y Genética. University of Salamanca. 37007-Salamanca, Spain.

[3]Department of Cellular and Molecular Biology. Centro de Investigaciones Biológicas Margarita Salas. Consejo Superior de Investigaciones Científicas (CSIC). 28040-Madrid, Spain

*Corresponding author: pedross@usal.es; +34 923294902

ORCID codes:

EH: 0000-0002-5839-6795

BS: 0000-0002-0781-0378

JAC: 0000-0003-2259-3743

PSS: 0000-0002-5616-574X

Keywords: meiosis, checkpoint, synapsis, recombination, Pch2, Hop1

ABSTRACT

During meiosis, defects in critical events trigger checkpoint activation and restrict cell cycle progression. The budding yeast Pch2 AAA+ ATPase orchestrates the checkpoint response launched by synapsis deficiency; deletion of *PCH2* or mutation of the ATPase catalytic sites suppress the meiotic block of the *zip1*Δ mutant lacking the central region of the synaptonemal complex. Pch2 action enables adequate levels of phosphorylation of the Hop1 axial component at threonine 318, which in turn promotes activation of the Mek1 effector kinase and the ensuing checkpoint response. In *zip1*Δ chromosomes, Pch2 is exclusively associated to the rDNA region, but this nucleolar fraction is not required for checkpoint activation, implying that another yet uncharacterized Pch2 population must be responsible for this function. Here, we have artificially redirected Pch2 to different subcellular compartments by adding ectopic NES or NLS sequences or by trapping Pch2 in an immobile extranuclear domain, and we have evaluated the effect on Hop1 chromosomal distribution and checkpoint activity. We have also deciphered the spatial and functional impact of Pch2 regulators including Orc1, Dot1 and Nup2. We conclude that the cytoplasmic pool of Pch2 is sufficient to support the meiotic recombination checkpoint involving the subsequent Hop1-Mek1 activation on chromosomes, whereas the nuclear accumulation of Pch2 has pathological consequences. We propose that cytoplasmic Pch2 provokes a conformational change in Hop1 that poises it for its chromosomal incorporation and phosphorylation. Our discoveries shed light into the intricate regulatory network controlling the accurate balance of Pch2 distribution among different cellular compartments, which is essential for proper meiotic outcomes.

INTRODUCTION

Sexually-reproducing organisms conduct a specialized type of cell division called meiosis. During this process, chromosome ploidy is reduced by half, due to two rounds of nuclear divisions preceded by only one round of DNA replication. Meiosis is characterized by its long prophase I stage, where the following highly regulated processes take place: pairing, synapsis and recombination. Recombination initiates with the introduction of programmed DNA double-strand breaks (DSBs) catalyzed by Spo11 and its associated proteins (Keeney et al., 2014). These breaks are then processed and repaired, part of them as crossovers (CO) (Allers and Lichten, 2001), to establish physical connections between homologous chromosomes essential to direct their proper segregation (San-Segundo and Clemente-Blanco, 2020). In parallel to recombination, chromosome synapsis occurs by the polymerization of the synaptonemal complex (SC) connecting the axes of paired homologs. This conserved highly-organized proteinaceous structure provides the adequate environment for properly regulated recombination. The SC comprises a central region, which in budding yeast is mainly composed by the transverse filament Zip1 protein (Sym et al., 1993) including also the so-called central element formed by Ecm11 and Gcm2 (Humphryes et al., 2013), and two lateral elements (LEs) made of Hop1, Red1 and Rec8 (Hollingsworth et al., 1990; Smith and Roeder, 1997; de los Santos and Hollingsworth, 1999; Klein et al., 1999; Lascarez-Lagunas et al., 2020a).

Progression and completion of these complex meiotic events are carefully monitored by a surveillance mechanism, called the meiotic recombination checkpoint, that triggers cell-cycle arrest in response to defective synapsis and/or recombination thus preventing meiotic chromosome missegregation (Subramanian and Hochwagen, 2014). Over the years, several components in this pathway have been identified using *S. cerevisiae* mutants defective in different meiotic events (i.e., *zip1Δ* or *dmc1Δ*) as genetic tools to activate the checkpoint. Current evidence indicates that the unique signal leading to checkpoint activation is the presence of unrepaired DSBs, and argues against the existence of a synapsis checkpoint in yeast (Hollingsworth and Gaglione, 2019). Moreover, a unified logic for the checkpoint response triggered both in the DSB repair-deficient *dmc1Δ* mutant and in the synapsis-defective *zip1Δ* mutant has been recently proposed (Raina and Vader, 2020). In these mutants, unrepaired resected meiotic DSBs recruit the Mec1^{ATR}-Ddc2^{ATRIP} kinase sensor complex (Refolio et al., 2011), which is responsible for Hop1^{HORMAD1,2} phosphorylation at various consensus S/T-Q sites. In particular, Red1-mediated Hop1 phosphorylation at T318 is required to recruit Mek1^{CHK2} to chromosome axes (Carballo et al., 2008; Chuang et al., 2012; Penedos et al.,

2015), thus favoring its dimerization and *trans* autophosphorylation events required for full Mek1 activation (Niu et al., 2005; Ontoso et al., 2013). In turn, activated Mek1 stabilizes Hop1-T318 phosphorylation in a positive feed-back loop (Chuang et al., 2012). In *zip1Δ*, The phosphorylation status of Hop1-T318 is critically modulated by the AAA+ ATPase Pch2^{TRIP13}, which is also responsible for Hop1 chromosomal abundance and dynamics (Herruzo et al., 2016) (see below). Once Mek1 is fully activated, it inhibits DSB repair by intersister recombination by preventing Rad54-Rad51 complex formation via direct phosphorylation of Rad54 and Hed1 (Niu et al., 2009; Callender et al., 2016). On the other hand, active Mek1 also blocks meiotic cell cycle progression by direct inhibition of Ndt80 (Chen et al., 2018), a transcription factor driving the expression of genes encoding proteins required for prophase I exit, such as the polo-like kinase Cdc5 and the type-B Clb1 cyclin (Chu and Herskowitz, 1998; Sourirajan and Lichten, 2008; Acosta et al., 2011). A negative feed-back loop has been described in which active Ndt80 downregulates Mek1 activity through Cdc5-dependent Red1 degradation (Prugar et al., 2017). Checkpoint-induced Mek1 activation also leads to high levels of the Swe1 kinase, which inhibits Cdc28^{CDK1} by phosphorylation at Tyr19, further contributing to slow down meiotic progression (Leu and Roeder, 1999; Gonzalez-Arranz et al., 2018).

Pch2 is an evolutionarily conserved AAA+ ATPase initially discovered in *S. cerevisiae* (San-Segundo and Roeder, 1999), but also present in other organisms that undergo synaptic meiosis such as worms, fruit flies, plants and mammals. Budding yeast Pch2 is meiosis specific and it has been implicated in a vast number of meiotic processes. The most thoroughly characterized role of Pch2 (known as TRIP13 in mammals) is the action on proteins that share a peptide-binding domain termed the HORMA domain (for Hop1, Rev7 and MAD2) (Vader, 2015). Since Hop1 is required for meiotic DSB formation, during wild-type meiosis Pch2^{TRIP13} excludes Hop1^{HORMAD1,2} from fully synapsed meiotic chromosomes, constituting a feedback mechanism suppressing further recombination on regions that have already synapsed (Wojtasz et al., 2009; Roig et al., 2010; Thacker et al., 2014; Subramanian et al., 2016). On the contrary, in the synapsis-defective *zip1Δ* mutant, Pch2 is critically required for the meiotic recombination checkpoint, promoting proper loading of Hop1 on unsynapsed chromosome axes and supporting sufficient levels of Hop1-T318 phosphorylation driving the downstream checkpoint response (Herruzo et al., 2016). In addition, in *C. elegans* and mammals, PCH-2^{TRIP13} also modulates the conformational state of MAD2 to accomplish a satisfactory spindle assembly checkpoint response (Nelson et al., 2015; Ye et al., 2015; Alfieri et al., 2018). As an AAA+ ATPase, Pch2 assembles into homo-hexamers with a central pore loop; this structure is critical for producing conformational changes on HORMA-containing proteins via cycles of nucleotide

binding and hydrolysis (Chen et al., 2014; Puchades et al., 2020). HORMAD proteins can assemble in multiprotein complexes through the binding of the HORMA domain core to the so-called closure motif in interacting partners. Both, the Hop1 binding partner Red1, and Hop1 itself, contain closure motifs that direct Hop1 assembly on chromosome axes (West et al., 2018; West et al., 2019). Furthermore, structural studies *in vitro* indicate that Hop1 can adopt two stable conformations in solution (West et al., 2018), similar to what is described for HORMAD proteins of higher eukaryotes (Kim et al., 2014; Ye et al., 2015; Ye et al., 2017). In the self-closed state of Hop1, the C-terminal closure motif bound to the HORMA domain is wrapped by the safety belt region located at the C-terminal part of the HORMA domain core, locking the closure motif. In the more extended conformation called 'unbuckled', the safety belt is disengaged allowing the binding to a new closure motif. It has been proposed that Pch2 catalyzes the transition from the "closed" to the "unbuckled" conformation releasing the safety belt lock from the HORMA domain core (West et al., 2018). Contrary to what is described in plants, worms and mammals, this action of Pch2 does not involve the p31^{COMET} co-factor, which is absent in budding yeast (Brulotte et al., 2017; Alfieri et al., 2018; Balboni et al., 2020; Giacopazzi et al., 2020).

Studies of budding yeast Pch2 localization on spread chromosomes have revealed that it mainly localizes to the rDNA region, but some foci are also detected on fully synapsed meiotic chromosomes (San-Segundo and Roeder, 1999; Joshi et al., 2009). This localization pattern differs in a synapsis-deficient situation that activates the checkpoint (i.e., *zip1Δ* mutant), where Pch2 loses its association to chromosomes and it is only concentrated on the nucleolar region (San-Segundo and Roeder, 1999; Herruzo et al., 2016). The presence of Pch2 in the rDNA, promoted by its interaction with Orc1, is required to exclude Hop1 from this region preventing potentially harmful DSB formation in this highly repetitive genomic location (San-Segundo and Roeder, 1999; Vader et al., 2011; Villar-Fernandez et al., 2020). Additional factors that regulate Pch2 distribution between the chromosomes and the rDNA are chromatin modifiers, such as the Dot1 histone methyltransferase and the Sir2 histone deacetylase (San-Segundo and Roeder, 1999; San-Segundo and Roeder, 2000; Vader et al., 2011; Ontoso et al., 2013; Cavero et al., 2016), the Nup2 nucleoporin (Subramanian et al., 2019), and the Top2 toposisomerase (Heldrich et al., 2020). We have recently demonstrated that Pch2 also shows a cytoplasmic localization, and that the Orc1-dependent nucleolar population of Pch2 is actually dispensable for the meiotic recombination checkpoint (Herruzo et al., 2019), leaving the prevention of DSB formation at the rDNA as the sole known role of nucleolar Pch2.

Here, we reveal where the population of Pch2 that is relevant for the *zip1*Δ-induced meiotic recombination checkpoint localizes in the cell. We show that in the *zip1*Δ *orc1-3mAID* mutant, Pch2 is exclusively detected in the cytoplasm and the checkpoint is fully active strongly suggesting that Pch2 promotes Hop1 association to unsynapsed meiotic chromosomes from the cytoplasm. Our analyses of the meiotic outcomes resulting from artificially forced nuclear import or export of Pch2, and from its sequestration at the inner face of the plasma membrane, further support the notion that the role of Pch2 in checkpoint activation is executed from outside the nucleus. We have also investigated the contribution of other proteins that control Pch2 localization. We demonstrate that when Pch2 is absent from the rDNA, Dot1 is no longer required for the checkpoint, indicating that the unique role of Dot1 in the meiotic recombination checkpoint is to maintain Pch2 nucleolar confinement to avoid harmful Pch2 accumulation on unsynapsed chromosomes. We additionally show that Nup2 also participates in Pch2 subcellular distribution; in the absence of Nup2, an increased cytoplasmic accumulation of Pch2 occurs and, consistently, the *zip1*Δ-induced checkpoint remains intact. In conclusion, we show for the first time the existence of a functionally relevant cytoplasmic pool of Pch2 in meiotic yeast cells and we define key requirements for a precise balance of Pch2 distribution among different subcellular compartments critical for successful meiotic function.

RESULTS

Pch2 localizes to the cytoplasm in the absence of Orc1, but the *zip1Δ*-induced checkpoint remains active.

Using chromosome spreading and a conditional auxin-inducible *orc1-3mAID* degron allele, we have previously described that Pch2 is not recruited to the nucleolus (rDNA) in the absence of Orc1; however, the *zip1Δ*-triggered meiotic recombination checkpoint remains fully functional in this situation, demonstrating that Pch2 nucleolar localization is dispensable for the checkpoint. Furthermore, in the *zip1Δ* mutant lacking Orc1, Pch2 is not detected whatsoever associated to meiotic chromosomes, but the meiotic checkpoint is still functional (Herruzo et al., 2019). This observation raises the possibility of a chromosome-independent fraction of Pch2 that may sustain the checkpoint response. To elucidate where the Pch2 population that is relevant for checkpoint function is present in the cell, we studied Pch2 localization in whole meiotic cells in different conditions. To this end, we used the P_{HOP1}-*GFP-PCH2* construct previously described expressing N-terminal GFP-tagged *PCH2* from the *HOP1* promoter

(Herruzo et al., 2019). All the *GFP-PCH2* variants employed throughout this paper are driven by the *HOP1* promoter, but for simplicity this feature is omitted from the relevant genotypes shown in the text and figures.

To examine Pch2 subcellular distribution in *zip1Δ orc1-3mAID* whole meiotic cells we integrated the *GFP-PCH2* construct into the genome at the *PCH2* locus. We first checked that the GFP-Pch2 protein is completely functional, as evidenced by the tight sporulation block of the *zip1Δ GFP-PCH2* strain, similar to that of *zip1Δ* (Figure 1A). Consistent with our previous results using strains harboring untagged or 3HA-tagged Pch2 (Herruzo et al., 2019), we confirmed that the checkpoint remains fully functional in the absence of Orc1; that is, in the *zip1Δ orc1-3mAID GFP-PCH2* strain treated with auxin. Checkpoint proficiency was manifested, in a prophase-arrested *ndt80Δ* background, by high levels of Hop1-T318 phosphorylation when Orc1 is depleted, also comparable to those of *zip1Δ* (Figure 1B). Next, we analyzed GFP-Pch2 and Hop1-mCherry subcellular distribution by fluorescence microscopy in live meiotic cells. Since Hop1-mCherry does not fully support checkpoint function, all the strains used in this work harboring *HOP1-mCherry* were heterozygous for this construct (*HOP1-mCherry*/*HOP1*). Using chromosome spreading we confirmed that in these heterozygous strains the Hop1 protein normally decorates chromosome axes and is excluded from the rDNA region (Figure S1). Furthermore, strains harboring *HOP1-mCherry* were only used for localization and staging purposes, not for functional analyses. In the *zip1Δ* mutant, GFP-Pch2 localized to a discrete region at one side of the nucleus that does not overlap with Hop1-mCherry. According with the well-characterized Pch2 localization on *zip1Δ* chromosome spreads (San-Segundo and Roeder, 1999; Herruzo et al., 2016; Herruzo et al., 2019), this discrete region corresponds to the nucleolus. In addition, GFP-Pch2 was also detected in the cytoplasm, displaying a diffuse homogenous signal (Figure 1C). In contrast, and consistent with the lack of Pch2 nucleolar localization upon Orc1 depletion observed by immunofluorescence of chromosome spreads (Vader et al., 2011; Herruzo et al., 2019), GFP-Pch2 exclusively localized to the cytoplasm in *zip1Δ orc1-3mAID* cells (Figure 1C). Quantification of the ratio between nuclear (including nucleolus) and cytoplasmic GFP signal confirmed the cytoplasmic accumulation of Pch2 in the absence of Orc1 (Figure 1D). Importantly, despite the altered subcellular distribution, total GFP-Pch2 protein levels were unaltered when Orc1 was depleted (Figure 1B). Since the checkpoint remains completely active in the *zip1Δ orc1-3mAID* mutant (Figure 1B) and checkpoint activity still depends on Pch2 (Herruzo et al., 2019), these results suggest that the cytoplasmic population of Pch2 is proficient to promote Hop1-Mek1 activation.

Redirecting Pch2 subcellular distribution

To further analyze how Pch2 subcellular distribution impacts on checkpoint function we fused a Nuclear Export Signal (NES) or a Nuclear Localization Signal (NLS) to Pch2 in order to force its localization outside or inside the nucleus, respectively. Canonical NES and NLS sequences were inserted between the *GFP* and *PCH2* coding sequences in centromeric plasmids containing the P_{HOP1}-*GFP-PCH2* construct (Figure S2A; see Materials and Methods for details). These plasmids were transformed into *zip1Δ* strains also harboring *HOP1-mCherry* as a marker both for the nucleus and for meiotic prophase stage. Live meiotic cells were analyzed by fluorescence microscopy to examine Pch2 localization. We found that, unlike the wild-type GFP-Pch2 protein, the GFP-NES-Pch2 version was largely excluded from the nucleolus and was almost exclusively present in the cytoplasm (Figure S2A, S2B). In contrast, GFP-NLS-Pch2 strongly accumulated in the nucleolus and also showed a diffuse pan-nuclear signal (Figure S2A, S2B). Thus, these constructs are useful tools to explore the effect of biased Pch2 subcellular localization.

To avoid issues derived from plasmid-loss events and from the inherent variability in plasmid copy number among individual cells in the culture, we generated strains in which the *GFP-PCH2* construct, as well as the *GFP-NES-PCH2* and *GFP-NLS-PCH2* derivatives, were integrated into the genome at the *PCH2* locus. We generated both homozygous (*GFP-PCH2/GFP-PCH2*) and heterozygous (*GFP-PCH2/pch2Δ*) versions of these diploid strains; the levels of GFP-Pch2 in the heterozygous strains (*het*) were more comparable to those of the endogenous Pch2, whereas the homozygous (*hom*) strains showed increased GFP-Pch2 amount (Figure 2A). We used these different variants to explore the impact of forced Pch2 localization on sporulation efficiency both in unperturbed meiosis and in checkpoint-inducing conditions; that is, in *ZIP1* and *zip1Δ* backgrounds, respectively. We found that, in *ZIP1* background, all GFP-Pch2, GFP-NES-Pch2 and GFP-NLS-Pch2 versions, when expressed either in homozygous or heterozygous strains, supported sporulation to the same levels as the wild type harboring untagged *PCH2* or the *pch2Δ* mutant did (Figure 2B, 2C; light grey bars). When we analyzed the impact of these Pch2 variants on *zip1Δ* strains, we found that sporulation was blocked in *zip1Δ GFP-PCH2* and *zip1Δ GFP-NES-PCH2*, both in the homozygous and heterozygous versions (Figure 2B, 2C). In contrast, the sporulation block was either slightly or largely released in the heterozygous or homozygous *zip1Δ GFP-NLS-PCH2* strains, respectively (Figure 2B, 2C; dark grey bars). These initial observations suggest that GFP-NES-Pch2 is checkpoint proficient, whereas increased dosage of GFP-NLS-Pch2 compromises

checkpoint function. We decided to use the heterozygous versions of all GFP-tagged *PCH2* constructs producing near physiological protein levels, as well as the homozygous *GFP-NLS-PCH2* (*hom*) for further comprehensive analyses of the functional impact of Pch2 localization.

We first thoroughly analyzed the subcellular localization of the different genomic-expressed GFP-tagged Pch2 versions in both *ZIP1* and *zip1Δ* live meiotic prophase I cells. Consistent with previous results using chromosome spreading, in *ZIP1* cells, the wild-type GFP-Pch2 was concentrated in a distinctive region inside the nucleus lacking Hop1-mCherry signal that corresponds to the nucleolus and, also, was detected in fainter discrete chromosomal foci. In addition, GFP-Pch2 displayed a diffuse cytoplasmic signal (Figure 3Aa; 3Ba). In the *zip1Δ* mutant, GFP-Pch2 was lost from the chromosomes and was only found in the nucleolus and cytoplasm (Figure 3Ab; 3Bb). In contrast, GFP-NES-Pch2 was mostly present in the cytoplasm in *ZIP1* and *zip1Δ* cells (Figure 3Ac,d; 3Bc,d); only a weak nucleolar signal remained in some cells, especially in the *ZIP1* strain (Figure 3Ac). In fact, quantification of the ratio between the nuclear (including nucleolus) and cytoplasmic GFP fluorescence revealed a significant reduction in this ratio in *GFP-NES-PCH2* strains compared to *GFP-PCH2* (Figure 3C). On the other hand, GFP-NLS-Pch2 was heavily accumulated in the nucleolus (Figure 3Ae,f; 3Be,f) and, in the case of *ZIP1* cells also in putative chromosomal foci (Figure 3Ae; 3Be); the nuclear/nucleolar accumulation was even more conspicuous in homozygous *GFP-NLS-PCH2* strains (Figure 3Ag-j; 3Bg-j; 3C). Interestingly, GFP-NLS-Pch2 was also diffusely localized in the nucleoplasm, particularly in homozygous *GFP-NLS-PCH2* cells (Figure 3Bj). Thus, the integrated GFP-NES-Pch2 variant drives the cytoplasmic accumulation of the protein, whereas GFP-NLS-Pch2 forces its localization inside the nucleus, predominantly, but not only, in the nucleolus.

We also quantified the Hop1-mCherry nuclear signal in all these situations with altered Pch2 localization (Figure 3D). In *ZIP1* strains, Hop1-mCherry levels were slightly increased in *GFP-NES-PCH2* cells, consistent with the notion that Pch2 was largely excluded from the nucleus/nucleolus and Hop1 eviction from synapsed chromosomes and the rDNA region would be impaired, as described (San-Segundo and Roeder, 1999; Borner et al., 2008; Herruzo et al., 2016). Consequently, NLS-driven nuclear accumulation of Pch2 resulted in reduced Hop1-mCherry levels both in *ZIP1* and *zip1Δ* strains. Curiously, the amount of nuclear Hop1-mCherry was also somewhat reduced in *zip1Δ GFP-NES-PCH2* cells despite the fact that Pch2 is not normally associated to unsynapsed chromosomes.

Differential effect of altered Pch2 subcellular distribution on Hop1 localization in synapsed versus unsynapsed chromosomes

To obtain more detailed information, we also analyzed the localization of GFP-Pch2, GFP-NES-Pch2 and GFP-NLS-Pch2, together with that of Hop1, on pachytene chromosome spreads from prophase-arrested *ndt80Δ* cells in both *ZIP1* and *zip1Δ* backgrounds. For clarity, we first describe the localization patterns in *ZIP1* cells. Consistent the known localization of Pch2 and the observations in live meiotic cells, the wild-type GFP-Pch2 protein localized mainly to the nucleolus (Figure 4Aa). As previously reported, the SC-associated Pch2 protein was barely detectable with this technique in the BR strain background (Herruzo et al., 2016; Herruzo et al., 2019) and only faint chromosomal GFP-Pch2 foci could be occasionally observed upon image overexposure (Figure S3). Nevertheless, in agreement with a normal distribution of Pch2 in synapsed *GFP-PCH2* nuclei, Hop1 displayed its characteristic weak and discontinuous signal, and was excluded from the nucleolus (Figure 4Aa). In *GFP-NES-PCH2* nuclei, Pch2 association to chromatin was largely lost and, accordingly, Hop1 displayed a more intense signal also moderately covering the rDNA region (Figure 4Ab; 4B; 4C), resembling the situation in the *pch2Δ* mutant (Figure 4Ae; 4C). In contrast, Pch2 densely decorated the nucleolar region in *GFP-NLS-PCH2* nuclei (Figure 4Ac) and the chromosomal foci were more visible, especially in the homozygous *GFP-NLS-PCH2* strain (Figure 4Ad). The increased presence of chromosome-associated GFP-NLS-Pch2 correlated with decreased abundance of Hop1 on spread nuclei (Figure 4B, 4C). Thus, in the context of synapsed chromosomes, the reduction of nuclear Pch2 (*GFP-NES-PCH2*) leads to increased Hop1 localization, including also the rDNA, like the complete lack of Pch2 (*pch2Δ*) does, whereas the nuclear accumulation of Pch2 (*GFP-NLS-PCH2*) counteracts Hop1 chromosomal localization.

We next describe the localization patterns of Hop1 and the different variants of GFP-tagged Pch2 in *zip1Δ* nuclei; that is, in a checkpoint-inducing condition. In *zip1Δ GFP-PCH2* nuclei, Pch2 was exclusively present in the nucleolus, and Hop1 showed the typical linear continuous pattern along unsynapsed axes, being excluded from the rDNA region (Figure 4Af). In turn, Pch2 was no longer present in the nucleolus in *zip1Δ GFP-NES-PCH2* nuclei, but Hop1 remained quite continuous along the axes also including the rDNA (Figure 4Ag). Thus, unlike the *zip1Δ pch2Δ* double mutant that displays discontinuous Hop1 localization even in the prophase-arrested *ndt80Δ* background (Figure 4Aj; (Herruzo et al., 2016)), the broad chromosomal (non rDNA) distribution of Hop1 in *zip1Δ* is not largely altered when Pch2 is forced out of the nucleus in *zip1Δ GFP-NES-PCH2*, arguing that, in *zip1Δ* nuclei, Pch2 is

capable of promoting proper axial Hop1 localization from its cytoplasmic location. However, although the pattern of Hop1 localization was not significantly altered in *zip1Δ GFP-NES-PCH2*, the intensity of Hop1 signal was reduced (Figure 4C), suggesting that Hop1 loading and/or turnover on the axes is compromised, perhaps due to residual Pch2 present in the nucleus during its transit towards the cytoplasm. On the other hand, *zip1Δ GFP-NLS-PCH2* nuclei exhibited a marked accumulation of Pch2 in the nucleolus (Figure 4Ah), but no Pch2 association with unsynapsed axes was detected even with higher Pch2 dosage (*zip1Δ GFP-NLS-PCH2* homozygous strain; Figure 4Ai). Despite that, Hop1 axial linearity and quantity was drastically diminished (Figure 4Ah,i; 4C) suggesting that the increased abundance of Pch2 inside the nucleus, specifically in the nucleoplasm (Figure 3Bj), drives Hop1 chromosomal removal and/or that the depletion of cytoplasmic Pch2 impairs Hop1 axial binding.

The predominantly cytoplasmic GFP-NES-Pch2 version supports checkpoint activity

To determine how Pch2 localization influences proper completion of meiosis we examined kinetics of meiotic nuclear divisions and spore viability in the strains harboring the variants of GFP-Pch2 with different subcellular and chromosomal distributions. Consistent with the fact that, in otherwise unperturbed meiosis, and at least in the BR strain background, the absence of Pch2 (*pch2Δ*) does not significantly affect meiotic progression, the kinetics of meiotic divisions of *GFP-NES-PCH2* and *GFP-NLS-PCH2* strains (in a *ZIP1* background) were almost indistinguishable to that of the wild-type *GFP-PCH2* strain (Figure 5A, top graph), despite having altered Pch2 localization (see above). Although Pch2 is involved in crossover control (Zanders and Alani, 2009), spore viability is high in the *pch2Δ* single mutant (Figure 5B, top graph). Accordingly, spore viability was not largely affected when the localization of Pch2 is altered (Figure 5B, top graph). Nevertheless, the influence of Pch2 in crossover homeostasis can be unveiled in situations, such as in *spo11* hypomorph mutants, where global DSB levels are reduced (Zanders and Alani, 2009; Carballo et al., 2013). Thus, we combined *GFP-PCH2, GFP-NES-PCH2* and *GFP-NLS-PCH2* with the *spo11-3HA* allele that confers about 80% of total DSB levels (Martini et al., 2006). As reported, spore viability decreased in the *pch2Δ spo11-3HA* double mutant, but it was normal in all heterozygous *GFP-PCH2, GFP-NES-PCH2* and *GFP-NLS-PCH2* strains harboring *spo11-3HA.* However, increased nuclear accumulation of Pch2 in the *GFP-NLS-PCH2* homozygous strain led to reduced spore viability in combination with *spo11-3HA* (Figure 5B, top graph). Like in *spo11-3HA pch2Δ*, the pattern of spore death in the *spo11-3HA GFP-NLS-PCH2* homozygous strain showed a trend to the

excess of tetrads with four-, two- and zero-viable spores, indicative of meiosis I nondisjunction events (Figure 5B, bottom graph; (Zanders and Alani, 2009)). Thus, curiously, both the complete lack of Pch2 or its forced strong accumulation inside the nucleus lead to the same pathological meiotic outcome.

We next studied the functionality of the different Pch2 versions in the context of checkpoint activation by *zip1Δ*. The *zip1Δ GFP-PCH2* diploid displayed a tight meiotic arrest (Figure 5A, bottom graph) further corroborating the notion that GFP-Pch2 is fully functional. Remarkably, the meiotic block triggered by the absence of Zip1 was almost fully maintained in *zip1Δ GFP-NES-PCH2* (Figure 5A, bottom graph) that largely lacks nuclear Pch2 and exhibits a predominantly cytoplasmic Pch2 localization. In turn, the meiotic arrest was released to some extent in the heterozygous *zip1Δ GFP-NLS-PCH2* mutant indicative of a somewhat weaker checkpoint response. Moreover, higher levels of nuclear Pch2 achieved in the homozygous *zip1Δ GFP-NLS-PCH2* strain led to a strong checkpoint defect, as manifested by the substantial alleviation of the meiotic arrest, almost equivalent to that of *zip1Δ pch2Δ* (Figure 5A, bottom graph).

Due to the different kinetics of meiotic progression conferred by the different GFP-Pch2 versions, particularly in a *zip1Δ* background (Figure 5A, bottom graph), we used prophase-arrested *ndt80Δ* strains for an accurate quantification of protein levels of Pch2, Hop1 and checkpoint markers (Figure 5C; 5D). We have previously reported that the critical function of Pch2 in the checkpoint triggered by defective synapsis is to sustain proper levels of Mec1-dependent Hop1-T318 phosphorylation required for the ensuing Mek1 activation (Herruzo et al., 2016). Thus, checkpoint activity supported by Pch2 was monitored by western blot analysis of phospho-Hop1-T318. Also, histone H3-T11 phosphorylation was determined as a proxy for Mek1 activation. Global levels of GFP-NES-Pch2 and GFP-NLS-Pch2 were only slightly reduced compared to GFP-Pch2 (Figure 5C; 5D), thus validating our localization studies (Figure 4). Like in the *pch2Δ* single mutant, Hop1 was more abundant in the *GFP-NES-PCH2* strain, compared to *GFP-PCH2* suggesting that the nuclear exclusion of Pch2 may lead to increased Hop1 protein stability on synapsed chromosomes. However, unlike *zip1Δ pch2Δ*, Hop1 global levels were similar in *zip1Δ GFP-PCH2* and *zip1Δ GFP-NES-PCH2* strains, suggesting than in the context of unsynapsed chromosomes, nuclear exclusion of Pch2 has no effect on Hop1 stability. On the other hand, forced nuclear localization of Pch2 (GFP-NLS-Pch2) resulted in a modest reduction of total Hop1 protein, primarily, in *zip1Δ* cells. Quantitative analysis of the levels of checkpoint markers (Hop1-T318 and H3-T11

phosphorylation) demonstrated that checkpoint activity was largely maintained in *zip1Δ GFP-NES-PCH2*, was reduced in *zip1Δ GFP-NLS-PCH2* heterozygous strains and was further compromised in *zip1Δ GFP-NLS-PCH2* homozygous strains (Figure 5C; 5D, dark grey bars).

Therefore, we conclude that the amount and distribution of Pch2 inside the nucleus must be carefully balanced to avoid deleterious effects on meiosis and, mainly, on the checkpoint response to defective synapsis (*zip1Δ*). In agreement with the analysis of the *orc1-3mAID* mutant (see above), these results also confirm that the cytoplasmic pool of Pch2 is proficient to sustain its checkpoint activation function.

Dot1 is irrelevant for the checkpoint when Pch2 is outside the nucleus

The histone H3K79 methyltransferase Dot1 is required for the checkpoint induced by the lack of Zip1; the absence of Dot1 suppresses the meiotic block of *zip1Δ*. Furthermore, deletion of *DOT1* (or mutation of H3K79) results in delocalization of Pch2 from the nucleolus and its general distribution throughout chromatin (San-Segundo and Roeder, 1999; Ontoso et al., 2013). These observations initially led to the hypothesis that the nucleolar localization of Pch2 may be important for its checkpoint function. However, we now have revealed a novel functionally-relevant cytoplasmic localization of Pch2 and we have demonstrated that the presence of Pch2 in the nucleolus is actually dispensable for the checkpoint (Herruzo et al., 2019); this work). Thus, to further delineate the functional impact of Dot1 action on Pch2 localization and checkpoint activity we analyzed the effect of deleting *DOT1* in those conditions where the checkpoint is still active but Pch2 is localized outside the nucleolus as a consequence of either Orc1 depletion (*zip1Δ orc1-3mAID GFP-PCH2*) or Pch2 fusion to a NES (*zip1Δ GFP-NES-PCH2*). Since the influence of Dot1 on Pch2 localization has been only studied using chromosome spreads, we examined wild-type GFP-Pch2 subcellular distribution in the absence of Dot1. We found that, consistent with previous reports, GFP-Pch2 relocalized from the nucleolus to pan-nuclear foci upon *DOT1* deletion in *zip1Δ* cells (Figure 6A). However, mutation of *DOT1* had no effect on the cytoplasmic distribution of Pch2 in *zip1Δ orc1-3mAID GFP-PCH2* or *zip1Δ GFP-NES-PCH2* cells; that is, Pch2 remained in the cytoplasm in those conditions (Figure 6A; 6B). To assess the status of checkpoint activity in these strains we analyzed sporulation efficiency, kinetics of meiotic nuclear divisions, and phosphorylation of Hop1-T318 and H3-T11. As expected, deletion of *DOT1* suppressed the sporulation arrest of *zip1Δ GFP-PCH2*. However, the *zip1Δ orc1-3mAID GFP-PCH2 dot1Δ* and *zip1Δ GFP-NES-PCH2 dot1Δ* mutants did not sporulate, suggesting that the checkpoint remains active in these

strains (Figure 6C). Moreover, like in *zip1Δ GFP-PCH2* and *zip1Δ orc1-3mAID GFP-PCH2*, meiotic progression in *zip1Δ orc1-3mAID GFP-PCH2 dot1Δ* was also completely blocked (Figure 6D), and high levels of Hop1-T318 and H3-T11 phosphorylation were maintained (Figure 6E), indicative of a robust checkpoint response. Nuclear divisions were also considerably delayed in *zip1Δ GFP-NES-PCH2 dot1Δ*, although a fraction of the cells resumed meiotic divisions at late time points (Figure 6D), and Hop1-T318 and H3-T11 phosphorylation also eventually declined (Figure 6E). This weaker checkpoint arrest in *zip1Δ GFP-NES-PCH2 dot1Δ* likely stems from the fact that a small amount of GFP-NES-Pch2 remains in the nucleolus in a fraction of cells expressing *GFP-NES-PCH2* (Figure 3A, 3B). Mislocalization and widespread distribution of this residual nucleolar GFP-NES-Pch2 population upon *DOT1* deletion would lead to the eventual partial loss of checkpoint strength.

We conclude that when Pch2 is depleted from the nucleolus and accumulates in the cytoplasm, Dot1 is no longer required to support meiotic checkpoint activity. Our results also indicate that the sole checkpoint function of Dot1-dependent H3K79 methylation is to maintain the nucleolar confinement of Pch2 to impede its pathological action on unsynapsed chromosomes. Thus, in terms of Pch2 localization, two requirements must be fulfilled in a *zip1Δ* mutant to elicit a proper checkpoint response: Pch2 must be present in the cytoplasm and the access of nuclear Pch2 to the chromosomes must be prevented. The latter is achieved by Dot1-dependent Pch2 restraint in the rDNA region.

Nup2 is not required for activation of the meiotic recombination checkpoint

Another factor influencing Pch2 localization is the Nup2 nucleoporin. It has been recently shown that, in wild-type (*ZIP1*) nuclei, Nup2 promotes the chromosomal localization of Pch2; the *nup2Δ* mutant exhibits an increased accumulation of Pch2 in the rDNA region at the expense of the chromosomal Pch2 fraction, resulting in an altered regional distribution of Hop1 (Subramanian et al., 2019). However, the impact of Nup2 on the subcellular localization of Pch2 and on the *zip1Δ*-induced checkpoint is not known. We first analyzed the localization of GFP-Pch2 in live meiotic cells lacking Nup2. Consistent with the previous report using chromosome spreading techniques (Subramanian et al., 2019), the GFP-Pch2 chromosomal foci were largely lost in the *nup2Δ* single mutant (Figure S4A). Also, an increase in the cytoplasmic fraction of GFP-Pch2 was observed in the absence of Nup2; this cytoplasmic accumulation was especially prominent in *zip1Δ nup2Δ* cells that also showed reduced nucleolar GFP-Pch2 signal compared to *zip1Δ* (Figure S4A; S4B; S4C). We then examined sporulation efficiency to assess

checkpoint functionality. Albeit with reduced efficiency, the *nup2Δ* single mutant sporulated; however, in contrast to *zip1Δ pch2Δ*, sporulation was completely blocked in the *zip1Δ nup2Δ* double mutant (Figure S4D). Thus, the checkpoint triggered by the absence of Zip1 is fully active in the *nup2Δ* mutant, which shows a conspicuous cytoplasmic Pch2 localization.

GFP-Pch2 tethering to the plasma membrane leads to constitutive checkpoint-dependent meiotic arrest

We have shown here that, in *zip1Δ orc1-3mAID GFP-PCH2* and *zip1Δ GFP-NES-PCH2* cells, the exclusive or preponderant, respectively, presence of Pch2 in the cytoplasm is sufficient to sustain meiotic checkpoint function. To further reinforce this notion and to explore whether Pch2 requires to be freely diffusible in the cytoplasm to exert its action, we took advantage of the GFP-binding protein (GBP) to tether GFP-NES-Pch2 (or GFP-Pch2) to a fixed cellular location outside the nucleus. In particular, we used a Pil1-GBP-mCherry fusion protein to force the localization of GFP-NES-Pch2 (or GFP-Pch2) to the eisosomes, which are immobile protein assemblies located at specialized domains of the plasma membrane. Pil1 is a major subunit of the eisosomes positioned at the cytoplasmic surface of the plasma membrane (Ziolkowska et al., 2011; Moseley, 2018). We generated *ZIP1* and *zip1Δ* strains harboring both *PIL1-GBP-mCherry* and *GFP-NES-PCH2*. As reported for eisosome localization, Pil1-GBP-mCherry formed quite uniform patches decorating the cellular periphery (Figure 7A). Remarkably, the GFP-NES-Pch2 protein was efficiently driven to the plasma membrane compartment containing Pil1-GBP-mCherry displaying a robust colocalization (Figure 7A; 7B). Not only the largely cytoplasmic GFP-NES-Pch2 protein was recruited to Pil1-GBP-mCherry patches; also, the wild-type GFP-Pch2 version was completely moved from its nuclear/nucleolar localization to the plasma membrane (Figure S5A). Highlighting the efficient sequestration of Pch2 at the plasma membrane, the Hop1 protein, which is normally excluded from the rDNA by Pch2 (Figure 4Af; Figure 7Ca), was conspicuously present in this region (identified by the nucleolar Nsr1 protein) in spread nuclei of *zip1Δ GFP-NES-PCH2 PIL1-GBP-mCherry* (Figure 7Cc) and *GFP-PCH2 PIL1-GBP-mCherry* (Figure S5B). Like in *zip1Δ GFP-PCH2* and *zip1Δ GFP-PCH2-NES* (Figure 7Ca,b), Hop1 also displayed a continuous and even stronger localization along unsynapsed axes in *zip1Δ GFP-NES-PCH2 PIL1-GBP-mCherry* (Figure 7Cc; 7D), contrasting with *zip1Δ pch2Δ* in which Hop1 linear localization is impaired (Herruzo et al., 2016); Figure 7Cd; 7D).

We next examined sporulation efficiency to assess checkpoint functionality. Like in *zip1Δ GFP-PCH2* and *zip1Δ GFP-NES-PCH2*, sporulation was blocked in the *zip1Δ GFP-NES-PCH2 PIL1-GBP-mCherry* strain (Figure 7E), indicating that the checkpoint is still active when Pch2 is anchored to the plasma membrane. Accordingly, high levels of Hop1-T318 and H3-T11 phosphorylation were maintained in *zip1Δ GFP-NES-PCH2 PIL1-GBP-mCherry* (Figure 7F). Unexpectedly, sporulation was also arrested, and high levels of active checkpoint markers were also achieved in otherwise wild-type cells (i.e., *ZIP1*) harboring *PIL1-GBP-mCherry* together with either *GFP-NES-PCH2* (Figure 7E, 7F) or *GFP-PCH2* (Figure S5C). This sporulation block was relieved by deletion of *MEK1* (Figure 7E; S5C) demonstrating that it resulted from activation of the meiotic recombination checkpoint. Thus, these results indicate not only that the checkpoint function of Pch2 is imposed from outside the nucleus, but also that immobilization of Pch2 in a fixed extranuclear compartment, namely the plasma membrane, leads to constitutive checkpoint activation. Furthermore, these observations also imply that Pch2 does not need to be freely diffusible in the cytoplasm to gain access to its substrate.

DISCUSSION

In this work we use different strategies to manipulate Pch2 localization within meiotic prophase I cells to establish the biological relevance, particularly for checkpoint function, of the presence of Pch2 in the different compartments where it can be located: unsynapsed rDNA region, synapsed chromosomes and cytoplasm. Since most, if not all, known meiotic events influenced by Pch2 activity occur in the nucleus, and the main Pch2 substrate, Hop1, is a component of chromosome axes, the majority of previous localization studies of Pch2 (and the orthologs in other organisms) have been exclusively focused on its chromosomal distribution. However, we have recently revealed that Pch2 also shows a diffuse cytoplasmic localization (Herruzo et al., 2019). Here, we demonstrate that the presence of Pch2 in the cytoplasm is essential for the checkpoint response to the absence of Zip1 and define the functional contribution of Pch2 regulators such as Orc1, Dot1 and Nup2 for a balanced distribution of Pch2 in different subcellular compartments. The most relevant observations relating Pch2 localization with Hop1 chromosomal pattern and checkpoint function in the different conditions analyzed are compiled in Table 1. A model for Pch2 action in the meiotic recombination checkpoint is presented in Figure 8 and Figure S6.

Activation of the meiotic recombination checkpoint relies on cytoplasmic Pch2

We have taken advantage of a functional version of Pch2 tagged with GFP to dissect the localization of Pch2 in whole meiotic cells. We have first analyzed GFP-Pch2 distribution upon Orc1 depletion. Orc1 recruits Pch2 to the rDNA region (Vader et al., 2011; Herruzo et al., 2019), but the absence of Orc1 does not alter the checkpoint response induced by *zip1Δ* indicating that the accumulation of Pch2 in the nucleolar region is only required to prevent recombination in the rDNA array (San-Segundo and Roeder, 1999; Vader et al., 2011), but it is dispensable for checkpoint activation (Herruzo et al., 2019). We show that GFP-Pch2 is only detected in the cytoplasm of *zip1Δ* meiotic cells lacking Orc1 indicating that Pch2 is capable of orchestrating the checkpoint response from this extra-nuclear location. Recent work using chromatin immunoprecipitation has proposed that, besides the rDNA, Orc1 also promotes Pch2 binding to a subset of RNA polymerase II-dependent actively transcribed genes (Cardoso da Silva et al., 2020). The biological relevance of this additional pool of euchromatin-associated Pch2 remains to be established, but several lines of evidence indicate that it is not involved in the *zip1Δ*-induced meiotic recombination checkpoint. First, recruitment of Pch2 to these transcribed genes is largely diminished in the absence of Zip1 (Cardoso da Silva et al., 2020), implying that another Pch2 population must perform the *zip1Δ*-induced checkpoint activation task. Second, the checkpoint is intact in the absence of Orc1, therefore, it does not rely on Orc1-mediated recruitment of Pch2 to anywhere in the genome, either heterochromatin (rDNA) or euchromatin (RNA polymerase II-transcribed genes). Third, although the crucial checkpoint role of Pch2 is to sustain Hop1-T318 phosphorylation (Herruzo et al., 2016), the binding of Pch2 to the body of actively transcribed genes has no impact whatsoever on Hop1 localization (Cardoso da Silva et al., 2020). Importantly, the checkpoint arrest of *zip1Δ orc1-3mAID* is alleviated by *PCH2* deletion (Herruzo et al., 2019) demonstrating that it does not stem from the activation of another independent meiotic surveillance mechanism and supporting the notion that Pch2 is still required for the checkpoint in this scenario acting from the cytoplasmic localization.

To further confirm the localization requirements of Pch2 for checkpoint activity we forced the accumulation of GFP-Pch2 inside or outside the nucleus by fusion to ectopic canonical NLS or NES sequences, respectively. Checkpoint function measured by various parameters is largely maintained in *zip1Δ GFP-NES-PCH2* cells that display a predominant cytoplasmic localization of Pch2 (Figure S6C). Although the majority of the GFP-NES-Pch2 protein is impelled towards the cytoplasm, some remnants can be still detected inside the

nucleus, especially in the nucleolus, likely accounting for the slightly weaker checkpoint arrest observed in *zip1Δ GFP-NES-PCH2*, compared to the absolute block of *zip1Δ orc1-3mAID* in which no hint of GFP-Pch2 is detected inside the nucleus. Conversely, NLS-mediated buildup of GFP-Pch2 inside the nucleus leads to checkpoint inactivation. Recent work has proposed that Pch2 possesses both a non-chromosomal checkpoint activating function and a chromosomal-dependent checkpoint-silencing function (Raina and Vader, 2020). Our results indicate that the non-chromosomal activating role of Pch2 is actually established in the cytoplasm. Moreover, we show that despite the large amount of Pch2 protein accumulated inside the nucleus in homozygous *zip1Δ GFP-NLS-PCH2* strains, it is only gathered in the nucleolus and also in the nucleoplasm, but it is not associated to (non-rDNA) unsynapsed chromosomes (Figures 3 and 4). This observation raises the possibility that the detrimental effect of nuclear Pch2 on checkpoint activity could be exerted even from the nucleoplasm (Figure S6D). Interestingly, the pathological effect of excessive nuclear Pch2 is not exclusive of the checkpoint response to unsynapsed chromosomes; in *ZIP1* strains harboring a hypomorphic *spo11-3HA* allele conferring reduced DSB levels, nuclear accumulation of GFP-NLS-Pch2 is also deleterious (Figure 5B), although in this case the effect may well be resulting from unrestrained Zip1-mediated recruitment of Pch2 to chromosomes.

Dot1 is exclusively required for Pch2 nucleolar confinement

Dot1-dependent H3K79me is required for the *zip1Δ* meiotic block triggered by the checkpoint (San-Segundo and Roeder, 2000; Ontoso et al., 2013). Surprisingly, we demonstrate here that when Pch2 is exclusively located outside the nucleus (i.e., in a *zip1Δ orc1-3mAID* mutant), Dot1 is no longer needed for the checkpoint. Since Pch2 loses the nucleolar confinement in *zip1Δ dot1Δ* cells and it is found throughout chromatin (Figure 6A; (San-Segundo and Roeder, 2000; Ontoso et al., 2013), the simplest interpretation is that Dot1 is solely required to maintain Pch2 sequestered in the rDNA chromatin preventing its nuclear dispersion and the subsequent negative action on checkpoint activity of widespread nuclear Pch2 (Figure S6E; S6F). We note that in the *zip1Δ dot1Δ* double mutant, Pch2 is capable of binding to unsynapsed chromosomes indicating that, in the absence of H3K79me, Pch2 can be recruited to chromosomes independently of Zip1. In fact, Pch2 is naturally recruited to the rDNA region, which is devoid of Zip1. We propose that global H3K79 methylation, likely full H3K79me3 (Ontoso et al., 2013), limits general Pch2 recruitment and that low levels of H3K79me in the rDNA allow Pch2 binding thus ensuring Pch2 confinement to the nucleolar

region. Dot1 activity is stimulated by H4K16 acetylation (Valencia-Sanchez et al., 2021). In prophase I meiotic nuclei, H4K16ac is widely distributed throughout chromatin, but it is excluded from the rDNA area (Cavero et al., 2016), thus supporting the notion that Dot1-dependent H3K79me should be reduced in the rDNA lacking H4K16ac. Pch2 binding to sites of active transcription shows some degree of correlation with H3K79me1 and it has been suggested that this modification may contribute to Orc1-dependent recruitment of Pch2 (Cardoso da Silva et al., 2020). Since the H3K79me1 isoform results from limited Dot1 catalytic activity (Frederiks et al., 2008); this observation may still be in agreement with the idea that full Dot1 enzymatic activity producing high levels of H3K79me3 prevents Pch2 binding. However, we note that the Orc1-driven transcription-associated Pch2 population is not involved in checkpoint regulation (see above), and that Pch2 is prominently recruited to unsynapsed chromosomes in the *dot1Δ* mutant lacking all forms of H3K79me, including H3K79me1.

Nup2 may promote Pch2 nuclear import

Nup2 is a mobile nucleoporin located in the basket of nuclear pore complexes (NPCs) that controls Hop1 retention in the so-called chromosome end-adjacent regions (EARs), which sustain continued meiotic DSB formation even after the establishment of the SC. Nup2 modulates Hop1 retention in the EARs by regulating Pch2 chromosomal distribution. Using chromosome spreading, it has been shown that, in the *nup2Δ* mutant, Pch2 chromosomal foci are greatly diminished, and most Pch2 concentrates in the nucleolar region (Subramanian et al., 2019). While our analysis of GFP-Pch2 localization in whole meiotic cells also reveals the absence of Pch2 chromosomal signal in *nup2Δ*, we do not detect a significant increase in the nucleolar signal (Figure S4C). This apparent discrepancy may result from the different detection technique or from certain peculiarities of the different strain background used. Indeed, the relative intensity of chromosomal and nucleolar Pch2 signal varies between wild-type BR and SK1 strains, with the chromosomal foci more easily detectable in SK1 (Joshi et al., 2009; Subramanian et al., 2016) and the nucleolar accumulation more prominent in BR (Herruzo et al., 2016; Herruzo et al., 2019). On the other hand, our results clearly show an increased cytoplasmic retention of GFP-Pch2 in the absence of Nup2; this cytoplasmic accumulation is particularly pronounced in the *zip1Δ nup2Δ* double mutant (Figure S4A). Consistent with the notion that the contribution of Pch2 to checkpoint activation in *zip1Δ* is established from the cytoplasm, sporulation is completely blocked in *zip1Δ nup2Δ* indicative of checkpoint

proficiency. Nup2 contains a denominated "meiotic autonomous region" that, in addition to the nuclear periphery, also localizes to foci on meiotic chromosomes (Chu et al., 2017). However, it is unlikely that Nup2 exerts a direct local control of Pch2 chromosomal distribution because, in *zip1Δ* cells, Pch2 is not recruited to chromosomes, but Pch2 subcellular distribution is still altered in the absence of Nup2. Since Nup2 is involved in the nuclear import of proteins in vegetative cells (Lange et al., 2020) and we find a cytoplasmic accumulation of Pch2 in *nup2Δ* mutants, we speculate that this nucleoporin may facilitate the entry and/or release of Pch2 into the nucleus via NPCs (Figure 8 and Figure S6G). Nevertheless, Nup2 is also involved in spatial organization of the genome (Brickner et al., 2019); therefore, an alternative or additional mode of Pch2 regulation by Nup2 within the nucleus, likely not involved in checkpoint activation, cannot be excluded.

Nucleocytoplasmic communication underlies meiotic checkpoint function

Our work highlights the relevance of nucleocytoplasmic traffic for the biology of meiosis; particularly, for the correct functionality of the meiotic recombination checkpoint. We propose that biochemical events occurring outside the nucleus have an impact on chromosomal transactions, namely Hop1 localization and phosphorylation. Since the only known substrate of Pch2 is the Hop1 protein, and the catalytic activity of Pch2 is required for the checkpoint (Herruzo et al., 2016), we postulate that Pch2 exerts an ATPase-dependent conformational change on Hop1 in the cytoplasm that poises it for its transport inside the nucleus, perhaps by exposing a cryptic NLS, and the subsequent Red1-dependent incorporation and Mec1-dependent phosphorylation on unsynapsed axes of the *zip1Δ* mutant (Figure 8 and Figure S6). It is likely that the conformational change involves the transition from the closed to the unbuckled conformation of Hop1 described *in vitro* (West et al., 2018), but the occurrence of this event remains to be demonstrated *in vivo*. Recent studies in *Arabidopsis thaliana* have also proposed a role for PCH2 in the nuclear transport of ASY1 (the Hop1 homolog) and posit that PCH2 would perform a second conformational change inside the nucleus, specifically in the nucleoplasm, required for the incorporation of ASY1 to the axial elements during early prophase I (Yang et al., 2020). We have shown that Hop1 axial localization is discontinuous in the *zip1*Δ *pch2*Δ mutant (Herruzo et al., 2016); Figure 4Aj; 7Cd), indicating that Pch2 is also required for efficient Hop1 incorporation on budding yeast unsynapsed chromosomes. However, we demonstrate here that the cytoplasmic Pch2 population is solely in charge of promoting efficient Hop1 loading: in *zip1Δ orc1-3mAID* and in *zip1Δ GFP-NES-PCH2 PIL1-*

GBP strains, Pch2 is exclusively localized outside the nucleus, and Hop1 displays a robust chromosomal linear pattern. Moreover, our results are in line with a recent report invoking a checkpoint silencing role for chromosomal Pch2 (Raina and Vader, 2020), because we show that the aberrant accumulation of Pch2 inside the nucleus (NLS-Pch2) or its unscheduled widespread chromatin incorporation in *zip1Δ dot1Δ* lead to checkpoint defects. Our striking observation that the tight tethering of Pch2 to the inner face of the plasma membrane leads to a constitutively active checkpoint response even in a synapsis-proficient context underscores the notion that, in this situation, only the extranuclear checkpoint activating function of Pch2 is manifested, whereas the nuclear silencing action is completely absent. It is likely that Pch2 always conducts the same biochemical transaction, namely Hop1 conversion from closed to unbuckled conformation, but depending on the subcellular location it causes opposite effects. Thus, the balance of Pch2 subcellular distribution and the dynamic communication among the different compartments must be strictly controlled for a proper meiotic recombination checkpoint response.

We envision that the emerging cytoplasmic function of Pch2 in the meiotic recombination checkpoint may be evolutionarily conserved. In *C. elegans*, PCH-2 localizes to pachytene chromosomes suggesting a direct local role for PCH-2 in regulating recombination, likely by unlocking HORMAD proteins in collaboration with the CMT-1 cofactor (Kim et al., 2014; Giacopazzi et al., 2020). However, worm PCH-2 is also required for the meiotic checkpoint induced in the synapsis-defective *syp-1* mutant (Bhalla and Dernburg, 2005). In this scenario, PCH-2 does not localize to chromosomes, opening the possibility that the diffuse extranuclear PCH-2 signal observed in *syp-1* (Deshong et al., 2014; Lascarez-Lagunas et al., 2020b), analogous to the cytoplasmic distribution of budding yeast Pch2 characterized here, may be relevant for the checkpoint in worms.

Together, our work provides new insights into fundamental determinants for Pch2 localization among the different compartments where the protein performs specialized functions. Remarkably, a plethora of distinct cellular mechanisms, including chromatin modifications and topology, nuclear transport, and replication factors, influences Pch2 regulation. Further understanding the interconnections in the regulatory network orchestrating the precise balance of Pch2 subcellular distribution and how it impinges on Hop1 status to ensure accurate completion of critical meiotic events will be an intriguing future venture.

MATERIALS AND METHODS

Yeast strains

The genotypes of yeast strains are listed in Table S1. All strains are in the BR1919 background (Rockmill and Roeder, 1990). The *zip1::LEU2*, *zip1::LYS2*, *ndt80::LEU2*, *ndt80::kanMX3*, *pch2::URA3, pch2::TRP1, dot1::URA3* and *dot1::kanMX6* gene deletions were previously described (San-Segundo and Roeder, 2000; Ontoso et al., 2013; Herruzo et al., 2016). The *mek1::natMX4* and *nup2::hphMX4* deletions were made using a PCR-based approach (Goldstein and McCusker, 1999). Strains harboring the *spo11-3HA-6His::kanMX4* allele were obtained by transforming cells with a 2.2-kb *Eco*RI-*Sac*II restriction fragment from pSK54 (Kee and Keeney, 2002). N-terminal tagging of Pch2 with three copies of the HA epitope, *HOP1-mCherry* tagging, and the *orc1-3mAID* construct have been previously described (San-Segundo and Roeder, 1999; Herruzo et al., 2019; Gonzalez-Arranz et al., 2020).

The P_{HOP1}*-GFP-PCH2* construct (Herruzo et al., 2019), as well as P_{HOP1}*-GFP-NES-PCH2* and P_{HOP1}*-GFP-NLS-PCH2,* were introduced into the genomic locus of *PCH2* using an adaptation of the *delitto perfetto* technique (Stuckey et al., 2011). Basically, PCR fragments flanked by the appropriate sequences were amplified from pSS393, pSS408 or pSS421 (see below), containing the *HOP1* promoter followed by the *GFP*, *GFP-NES* or *GFP-NLS* sequences, respectively, and a five Gly-Ala repeat linker before the second codon of *PCH2*. These fragments were transformed into a strain carrying the CORE cassette (*kanMX4-URA3*) inserted close to the 5' end of *PCH2*. G418-sensitive and 5-FOA-resistant clones containing the correct integrated construct, which results in the elimination of 91 nt of the *PCH2* promoter, were checked by PCR and verified by sequencing.

PIL1-GBP-mCherry strains were made following a normal PCR-based strategy for C-terminal tagging using a pFA6a-derived vector (pSS383) containing *GBP-mCherry::hphMX6*, kindly provided by A. Fernández-Álvarez (UPO, Sevilla).

All constructions and mutations were verified by PCR analysis and/or sequencing. The sequences of all primers used in strain construction are available upon request. All strains were made by direct transformation of haploid parents or by genetic crosses always in an isogenic background. Diploids were made by mating the corresponding haploid parents and isolation of zygotes by micromanipulation.

Plasmids

The plasmids used are listed in Table S2. The pSS393 centromeric plasmid expressing P_{HOP1}-*GFP-PCH2* was previously described (Herruzo et al., 2019). The pSS408 and pSS421 plasmids driving the expression of P_{HOP1}-*GFP-NES-PCH2* and P_{HOP1}-*GFP-NLS-PCH2,* respectively, were derived from pSS393. An approximately 350 bp fragment corresponding to N-terminal region of *PCH2* was amplified from pSS393 with forward primers encoding the canonical NES (LALKLAGLDI) (Wen et al., 1995) or NLS (PKKKRKV) (Kalderon et al., 1984) sequences preceded by a *Not*I site at the 5' end, and a reverse primer within the *PCH2* coding sequence downstream of the endogenous *Bam*HI site. These fragments were digested with *Not*I-*Bam*HI and cloned into the same sites of pSS393.

Meiotic cultures and meiotic time courses

To induce meiosis and sporulation, BR strains were grown in 3.5 ml of synthetic complete medium (2% glucose, 0.7% yeast nitrogen base without amino acids, 0.05% adenine, and complete supplement mixture from Formedium at twice the particular concentration indicated by the manufacturer) for 20–24 h, then transferred to 2.5 ml of YPDA (1% yeast extract, 2% peptone, 2% glucose, and 0.02% adenine) and incubated to saturation for an additional 8 h. Cells were harvested, washed with 2% potassium acetate (KAc), resuspended into 2% KAc (10 ml), and incubated at 30°C with vigorous shaking to induce meiosis. Both YPDA and 2% KAc were supplemented with 20 mM adenine and 10 mM uracil. The culture volumes were scaled up when needed. To induce Orc1-3mAID degradation, auxin (500µM) was added to the cultures 12 h after meiotic induction.

To score meiotic nuclear divisions, samples from meiotic cultures were taken at different time points, fixed in 70% ethanol, washed in phosphate-buffered saline (PBS) and stained with 1 µg/µl 4′,6-diamidino-2- phenylindole (DAPI) for 15 min. At least 300 cells were counted at each time point. Meiotic time courses were repeated several times; averages and error bars from at least three replicates are shown.

Western blotting

Total cell extracts for Western blot analysis were prepared by trichloroacetic acid (TCA) precipitation from 5-ml aliquots of sporulation cultures, as previously described (Acosta et al., 2011). The antibodies used are listed in Table S3. The ECL, ECL2 or SuperSignal West Femto reagents (ThermoFisher Scientific) were used for detection. The signal was captured on films and/or with a Fusion FX6 system (Vilber) and quantified with the Evolution-Capt software (Vilber).

Cytology

Immunofluorescence of chromosome spreads was performed essentially as described (Rockmill, 2009). The antibodies used are listed in Supplementary Table S3. Images of spreads were captured with a Nikon Eclipse 90i fluorescence microscope controlled with MetaMorph software (Molecular Devices) and equipped with a Hammamatsu Orca-AG charge-coupled device (CCD) camera and a PlanApo VC 100x 1.4 NA objective. Images of whole live cells expressing *GFP-PCH2*, *HOP1-mCherry* and *PIL1-GBP-mCherry* were captured with an Olympus IX71 fluorescence microscope equipped with a personal DeltaVision system, a CoolSnap HQ2 (Photometrics) camera, and 100x UPLSAPO 1.4 NA objective. Stacks of 7 planes at 0.8-µm intervals were collected. Maximum intensity projections of 3 planes containing Hop1-mCherry signal and single planes of GFP-Pch2 are shown in Figures 1C; 3A; 3B; 6A; S2A and S4A. In Figures 7A and S5A, a single plane of Pil1-mCherry and GFP-Pch2 is shown. The line-scan tool of the MetaMorph software was used to measure and plot the fluorescence intensity profile across the cell in Figure 7B. To determine the nuclear/cytoplasm GFP fluorescence ratio, the ROI manager tool of Fiji software (Schindelin et al., 2012) was used to define the cytoplasm and nuclear (including the nucleolus) areas and the mean intensity values were measured. The Hop1-mCherry signal in whole cells was measured by using the same system but defining only the nuclear region. On the other hand, to determine the nucleolar GFP-Pch2 intensity, only the nucleolus was defined based on the conspicuous GFP-Pch2 structure restricted to one side of the nucleus. To determine Pch2 and Hop1 intensity on chromosome spreads, a region containing DAPI-stained chromatin was defined and the Raw Integrated Density values were measured. Background values were subtracted prior to ratio calculation. For background subtraction, the rolling ball algorithm from Fiji was used setting the radius to 50 pixels.

Dityrosine fluorescence assay, sporulation efficiency, and spore viability

To examine dityrosine fluorescence as an indicator of the formation of mature asci, patches of cells grown on YPDA plates were replica-plated to sporulation plates overlaid with a nitrocellulose filter (Protran BA85, Whatman). After 3-day incubation at 30 °C, fluorescence was visualized by illuminating the open plates from the top with a hand-held 302-nm ultraviolet (UV) lamp. Images were taken using a Gel Doc XR system (Bio-Rad). Sporulation efficiency was quantitated by microscopic examination of asci formation after 3 days on sporulation plates. Both mature and immature asci were scored. At least 300 cells were counted for every

strain. Spore viability was assessed by tetrad dissection. At least 216 spores were scored for every strain.

Statistics

To determine the statistical significance of differences, a two-tailed Student t-test was used. *P*-values were calculated with the GraphPad Prism 8.0 software. The nature of the error bars in the graphical representations and the number of biological replicates are indicated in the corresponding figure legend.

ACKNOWLEDGEMENTS

We are grateful to Andrés Clemente, David Álvarez-Melo and Félix Prado for helpful comments and discussions. We also thank Alfonso Fernández-Álvarez, Andrés Clemente and Scott Keeney for reagents, and Sara González-Arranz and Carlos R. Vázquez for advice on microscopy analysis. This work was supported by the grant RTI2018-099055-B-I00 from Ministry of Science, Innovation and Universities (MCIU/AEI/FEDER, EU) of Spain to PSS and JAC. EH was partially supported by the grant CSI259P20 from the "Junta de Castilla y León". The IBFG is supported in part by an institutional grant from the "Junta de Castilla y León, Ref. CLU-2017-03 co-funded by the P.O. FEDER de Castilla y León 14-20".

AUTHOR CONTRIBUTIONS

EH: conceptualization, investigation, formal analysis, visualization.
ALM: investigation, formal analysis.
SB: investigation.
BS: supervision, project administration.
JAC: conceptualization, resources, funding acquisition.
PSS: conceptualization, investigation, supervision, funding acquisition, visualization, writing original draft.

All authors revised, commented and approved the manuscript.

Conflict of Interest: The authors declare that they have no conflict of interest.

REFERENCES

Acosta, I., D. Ontoso, and P.A. San-Segundo. 2011. The budding yeast polo-like kinase Cdc5 regulates the Ndt80 branch of the meiotic recombination checkpoint pathway. *Mol Biol Cell*. 22:3478-3490.

Alfieri, C., L. Chang, and D. Barford. 2018. Mechanism for remodelling of the cell cycle checkpoint protein MAD2 by the ATPase TRIP13. *Nature*. 559:274-278.

Allers, T., and M. Lichten. 2001. Differential timing and control of noncrossover and crossover recombination during meiosis. *Cell*. 106:47-57.

Balboni, M., C. Yang, S. Komaki, J. Brun, and A. Schnittger. 2020. COMET Functions as a PCH2 Cofactor in Regulating the HORMA Domain Protein ASY1. *Curr Biol*. 30:4113-4127 e4116.

Bhalla, N., and A.F. Dernburg. 2005. A conserved checkpoint monitors meiotic chromosome synapsis in *Caenorhabditis elegans*. *Science*. 310:1683-1686.

Borner, G.V., A. Barot, and N. Kleckner. 2008. Yeast Pch2 promotes domainal axis organization, timely recombination progression, and arrest of defective recombinosomes during meiosis. *Proc Natl Acad Sci USA*. 105:3327-3332.

Brickner, D.G., C. Randise-Hinchliff, M. Lebrun Corbin, J.M. Liang, S. Kim, B. Sump, A. D'Urso, S.H. Kim, A. Satomura, H. Schmit, R. Coukos, S. Hwang, R. Watson, and J.H. Brickner. 2019. The Role of Transcription Factors and Nuclear Pore Proteins in Controlling the Spatial Organization of the Yeast Genome. *Dev Cell*. 49:936-947 e934.

Brulotte, M.L., B.C. Jeong, F. Li, B. Li, E.B. Yu, Q. Wu, C.A. Brautigam, H. Yu, and X. Luo. 2017. Mechanistic insight into TRIP13-catalyzed Mad2 structural transition and spindle checkpoint silencing. *Nat Commun*. 8:1956.

Callender, T.L., R. Laureau, L. Wan, X. Chen, R. Sandhu, S. Laljee, S. Zhou, R.T. Suhandynata, E. Prugar, W.A. Gaines, Y. Kwon, G.V. Borner, A. Nicolas, A.M. Neiman, and N.M. Hollingsworth. 2016. Mek1 Down Regulates Rad51 Activity during Yeast Meiosis by Phosphorylation of Hed1. *PLoS Genet*. 12:e1006226.

Carballo, J.A., A.L. Johnson, S.G. Sedgwick, and R.S. Cha. 2008. Phosphorylation of the axial element protein Hop1 by Mec1/Tel1 ensures meiotic interhomolog recombination. *Cell*. 132:758-770.

Carballo, J.A., S. Panizza, M.E. Serrentino, A.L. Johnson, M. Geymonat, V. Borde, F. Klein, and R.S. Cha. 2013. Budding yeast ATM/ATR control meiotic double-strand break (DSB) levels by down-regulating Rec114, an essential component of the DSB-machinery. *PLoS Genet*. 9:e1003545.

Cardoso da Silva, R., M.A. Villar-Fernandez, and G. Vader. 2020. Active transcription and Orc1 drive chromatin association of the AAA+ ATPase Pch2 during meiotic G2/prophase. *PLoS Genet*. 16:e1008905.

Cavero, S., E. Herruzo, D. Ontoso, and P.A. San-Segundo. 2016. Impact of histone H4K16 acetylation on the meiotic recombination checkpoint in Saccharomyces cerevisiae. *Microb Cell*. 3:606-620.

Chen, C., A. Jomaa, J. Ortega, and E.E. Alani. 2014. Pch2 is a hexameric ring ATPase that remodels the chromosome axis protein Hop1. *Proc Natl Acad Sci USA*. 111:E44-53.

Chen, X., R. Gaglione, T. Leong, L. Bednor, T. de Los Santos, E. Luk, M. Airola, and N.M. Hollingsworth. 2018. Mek1 coordinates meiotic progression with DNA break repair by directly phosphorylating and inhibiting the yeast pachytene exit regulator Ndt80. *PLoS Genet*. 14:e1007832.

Chu, D.B., T. Gromova, T.A.C. Newman, and S.M. Burgess. 2017. The Nucleoporin Nup2 Contains a Meiotic-Autonomous Region that Promotes the Dynamic Chromosome Events of Meiosis. *Genetics*. 206:1319-1337.

Chu, S., and I. Herskowitz. 1998. Gametogenesis in yeast is regulated by a transcriptional cascade dependent on Ndt80. *Mol Cell*. 1:685-696.

Chuang, C.N., Y.H. Cheng, and T.F. Wang. 2012. Mek1 stabilizes Hop1-Thr318 phosphorylation to promote interhomolog recombination and checkpoint responses during yeast meiosis. *Nucleic Acids Res*. 40:11416-11427.

de los Santos, T., and N.M. Hollingsworth. 1999. Red1p, a MEK1-dependent phosphoprotein that physically interacts with Hop1p during meiosis in yeast. *J Biol Chem*. 274:1783-1790.

Deshong, A.J., A.L. Ye, P. Lamelza, and N. Bhalla. 2014. A quality control mechanism coordinates meiotic prophase events to promote crossover assurance. *PLoS Genet*. 10:e1004291.

Frederiks, F., M. Tzouros, G. Oudgenoeg, T. van Welsem, M. Fornerod, J. Krijgsveld, and F. van Leeuwen. 2008. Nonprocessive methylation by Dot1 leads to functional redundancy of histone H3K79 methylation states. *Nat Struct Mol Biol*. 15:550-557.

Giacopazzi, S., D. Vong, A. Devigne, and N. Bhalla. 2020. PCH-2 collaborates with CMT-1 to proofread meiotic homolog interactions. *PLoS Genet*. 16:e1008904.

Goldstein, A.L., and J.H. McCusker. 1999. Three new dominant drug resistance cassettes for gene disruption in *Saccharomyces cerevisiae*. *Yeast*. 15:1541-1553.

Gonzalez-Arranz, S., S. Cavero, M. Morillo-Huesca, E. Andujar, M. Perez-Alegre, F. Prado, and P. San-Segundo. 2018. Functional Impact of the H2A.Z Histone Variant During Meiosis in Saccharomyces cerevisiae. *Genetics*. 209:997-1015.

Gonzalez-Arranz, S., J.M. Gardner, Z. Yu, N.J. Patel, J. Heldrich, B. Santos, J.A. Carballo, S.L. Jaspersen, A. Hochwagen, and P.A. San-Segundo. 2020. SWR1-Independent Association of H2A.Z to the LINC Complex Promotes Meiotic Chromosome Motion. *Front Cell Dev Biol*. 8:594092.

Heldrich, J., X. Sun, L.A. Vale-Silva, T.E. Markowitz, and A. Hochwagen. 2020. Topoisomerases Modulate the Timing of Meiotic DNA Breakage and Chromosome Morphogenesis in *Saccharomyces cerevisiae*. *Genetics*. 215:59-73.

Herruzo, E., D. Ontoso, S. Gonzalez-Arranz, S. Cavero, A. Lechuga, and P.A. San-Segundo. 2016. The Pch2 AAA+ ATPase promotes phosphorylation of the Hop1 meiotic checkpoint adaptor in response to synaptonemal complex defects. *Nucleic Acids Res*. 44:7722-7741.

Herruzo, E., B. Santos, R. Freire, J.A. Carballo, and P.A. San-Segundo. 2019. Characterization of Pch2 localization determinants reveals a nucleolar-independent role in the meiotic recombination checkpoint. *Chromosoma*. 128:297-316.

Hollingsworth, N.M., and R. Gaglione. 2019. The meiotic-specific Mek1 kinase in budding yeast regulates interhomolog recombination and coordinates meiotic progression with double-strand break repair. *Curr Genet*. 65:631-641.

Hollingsworth, N.M., L. Goetsch, and B. Byers. 1990. The HOP1 gene encodes a meiosis-specific component of yeast chromosomes. *Cell*. 61:73-84.

Humphryes, N., W.K. Leung, B. Argunhan, Y. Terentyev, M. Dvorackova, and H. Tsubouchi. 2013. The Ecm11-Gmc2 complex promotes synaptonemal complex formation through assembly of transverse filaments in budding yeast. *PLoS Genet*. 9:e1003194.

Joshi, N., A. Barot, C. Jamison, and G.V. Borner. 2009. Pch2 links chromosome axis remodeling at future crossover sites and crossover distribution during yeast meiosis. *PLoS Genet*. 5:e1000557.

Kalderon, D., B.L. Roberts, W.D. Richardson, and A.E. Smith. 1984. A short amino acid sequence able to specify nuclear location. *Cell*. 39:499-509.

Kee, K., and S. Keeney. 2002. Functional interactions between SPO11 and REC102 during initiation of meiotic recombination in *Saccharomyces cerevisiae*. *Genetics*. 160:111-122.

Keeney, S., J. Lange, and N. Mohibullah. 2014. Self-organization of meiotic recombination initiation: general principles and molecular pathways. *Annu Rev Genet*. 48:187-214.

Kim, Y., S.C. Rosenberg, C.L. Kugel, N. Kostow, O. Rog, V. Davydov, T.Y. Su, A.F. Dernburg, and K.D. Corbett. 2014. The chromosome axis controls meiotic events through a hierarchical assembly of HORMA domain proteins. *Dev Cell*. 31:487-502.

Klein, F., P. Mahr, M. Galova, S.B. Buonomo, C. Michaelis, K. Nairz, and K. Nasmyth. 1999. A central role for cohesins in sister chromatid cohesion, formation of axial elements, and recombination during yeast meiosis. *Cell*. 98:91-103.

Lange, A., M.B. Fasken, M. Stewart, and A.H. Corbett. 2020. Dissecting the roles of Cse1 and Nup2 in classical NLS-cargo release in vivo. *Traffic*. 21:622-635.

Lascarez-Lagunas, L., M. Martinez-Garcia, and M. Colaiacovo. 2020a. SnapShot: Meiosis - Prophase I. *Cell*. 181:1442-1442 e1441.

Lascarez-Lagunas, L.I., E. Herruzo, A. Grishok, P.A. San-Segundo, and M.P. Colaiacovo. 2020b. DOT-1.1-dependent H3K79 methylation promotes normal meiotic progression and meiotic checkpoint function in *C. elegans*. *PLoS Genet*. 16:e1009171.

Leu, J.Y., and G.S. Roeder. 1999. The pachytene checkpoint in *S. cerevisiae* depends on Swe1-mediated phosphorylation of the cyclin-dependent kinase Cdc28. *Mol Cell*. 4:805-814.

Martini, E., R.L. Diaz, N. Hunter, and S. Keeney. 2006. Crossover homeostasis in yeast meiosis. *Cell*. 126:285-295.

Moseley, J.B. 2018. Eisosomes. *Curr Biol*. 28:R376-R378.

Nelson, C.R., T. Hwang, P.H. Chen, and N. Bhalla. 2015. TRIP13PCH-2 promotes Mad2 localization to unattached kinetochores in the spindle checkpoint response. *J Cell Biol*. 211:503-516.

Niu, H., L. Wan, B. Baumgartner, D. Schaefer, J. Loidl, and N.M. Hollingsworth. 2005. Partner choice during meiosis is regulated by Hop1-promoted dimerization of Mek1. *Mol Biol Cell*. 16:5804-5818.

Niu, H., L. Wan, V. Busygina, Y. Kwon, J.A. Allen, X. Li, R.C. Kunz, K. Kubota, B. Wang, P. Sung, K.M. Shokat, S.P. Gygi, and N.M. Hollingsworth. 2009. Regulation of meiotic recombination via Mek1-mediated Rad54 phosphorylation. *Mol Cell*. 36:393-404.

Ontoso, D., I. Acosta, F. van Leeuwen, R. Freire, and P.A. San-Segundo. 2013. Dot1-dependent histone H3K79 methylation promotes activation of the Mek1 meiotic checkpoint effector kinase by regulating the Hop1 adaptor. *PLoS Genet*. 9:e1003262.

Penedos, A., A.L. Johnson, E. Strong, A.S. Goldman, J.A. Carballo, and R.S. Cha. 2015. Essential and Checkpoint Functions of Budding Yeast ATM and ATR during Meiotic Prophase Are Facilitated by Differential Phosphorylation of a Meiotic Adaptor Protein, Hop1. *PLoS One*. 10:e0134297.

Prugar, E., C. Burnett, X. Chen, and N.M. Hollingsworth. 2017. Coordination of Double Strand Break Repair and Meiotic Progression in Yeast by a Mek1-Ndt80 Negative Feedback Loop. *Genetics*. 206:497-512.

Puchades, C., C.R. Sandate, and G.C. Lander. 2020. The molecular principles governing the activity and functional diversity of AAA+ proteins. *Nat Rev Mol Cell Biol*. 21:43-58.

Raina, V.B., and G. Vader. 2020. Homeostatic Control of Meiotic Prophase Checkpoint Function by Pch2 and Hop1. *Curr Biol*. 30:4413-4424 e4415.

Refolio, E., S. Cavero, E. Marcon, R. Freire, and P.A. San-Segundo. 2011. The Ddc2/ATRIP checkpoint protein monitors meiotic recombination intermediates *J Cell Sci*. 124:2488-2500.

Rockmill, B. 2009. Chromosome spreading and immunofluorescence methods in *Saccharomyes cerevisiae*. *Methods Mol Biol*. 558:3-13.

Rockmill, B., and G.S. Roeder. 1990. Meiosis in asynaptic yeast. *Genetics*. 126:563-574.

Roig, I., J.A. Dowdle, A. Toth, D.G. de Rooij, M. Jasin, and S. Keeney. 2010. Mouse TRIP13/PCH2 is required for recombination and normal higher-order chromosome structure during meiosis. *PLoS Genet*. 6:e1001062.

San-Segundo, P.A., and A. Clemente-Blanco. 2020. Resolvases, Dissolvases, and Helicases in Homologous Recombination: Clearing the Road for Chromosome Segregation. *Genes*. 11:71.

San-Segundo, P.A., and G.S. Roeder. 1999. Pch2 links chromatin silencing to meiotic checkpoint control. *Cell*. 97:313-324.

San-Segundo, P.A., and G.S. Roeder. 2000. Role for the silencing protein Dot1 in meiotic checkpoint control. *Mol Biol Cell*. 11:3601-3615.

Schindelin, J., I. Arganda-Carreras, E. Frise, V. Kaynig, M. Longair, T. Pietzsch, S. Preibisch, C. Rueden, S. Saalfeld, B. Schmid, J.Y. Tinevez, D.J. White, V. Hartenstein, K. Eliceiri, P. Tomancak, and A. Cardona. 2012. Fiji: an open-source platform for biological-image analysis. *Nat Methods*. 9:676-682.

Smith, A.V., and G.S. Roeder. 1997. The yeast Red1 protein localizes to the cores of meiotic chromosomes. *J Cell Biol*. 136:957-967.

Sourirajan, A., and M. Lichten. 2008. Polo-like kinase Cdc5 drives exit from pachytene during budding yeast meiosis. *Genes Dev*. 22:2627-2632.

Stuckey, S., K. Mukherjee, and F. Storici. 2011. In vivo site-specific mutagenesis and gene collage using the delitto perfetto system in yeast Saccharomyces cerevisiae. *Methods Mol Biol*. 745:173-191.

Subramanian, V.V., and A. Hochwagen. 2014. The Meiotic Checkpoint Network: Step-by-Step through Meiotic Prophase. *Cold Spring Harbor perspectives in biology*. 6:a016675.

Subramanian, V.V., A.J. MacQueen, G. Vader, M. Shinohara, A. Sanchez, V. Borde, A. Shinohara, and A. Hochwagen. 2016. Chromosome Synapsis Alleviates Mek1-Dependent Suppression of Meiotic DNA Repair. *PLoS Biol*. 14:e1002369.

Subramanian, V.V., X. Zhu, T.E. Markowitz, L.A. Vale-Silva, P.A. San-Segundo, N.M. Hollingsworth, S. Keeney, and A. Hochwagen. 2019. Persistent DNA-break potential near telomeres increases initiation of meiotic recombination on short chromosomes. *Nat Commun*. 10:970.

Sym, M., J.A. Engebrecht, and G.S. Roeder. 1993. ZIP1 is a synaptonemal complex protein required for meiotic chromosome synapsis. *Cell*. 72:365-378.

Thacker, D., N. Mohibullah, X. Zhu, and S. Keeney. 2014. Homologue engagement controls meiotic DNA break number and distribution. *Nature*. 510:241-246.

Vader, G. 2015. Pch2(TRIP13): controlling cell division through regulation of HORMA domains. *Chromosoma*. 124:333-339.

Vader, G., H.G. Blitzblau, M.A. Tame, J.E. Falk, L. Curtin, and A. Hochwagen. 2011. Protection of repetitive DNA borders from self-induced meiotic instability. *Nature*. 477:115-119.

Valencia-Sanchez, M.I., P. De Ioannes, M. Wang, D.M. Truong, R. Lee, J.P. Armache, J.D. Boeke, and K.J. Armache. 2021. Regulation of the Dot1 histone H3K79 methyltransferase by histone H4K16 acetylation. *Science*. 371:eabc6663.

Villar-Fernandez, M.A., R. Cardoso da Silva, M. Firlej, D. Pan, E. Weir, A. Sarembe, V.B. Raina, T. Bange, J.R. Weir, and G. Vader. 2020. Biochemical and functional characterization of a meiosis-specific Pch2/ORC AAA+ assembly. *Life Sci Alliance*. 3:e201900630.

Wen, W., J.L. Meinkoth, R.Y. Tsien, and S.S. Taylor. 1995. Identification of a signal for rapid export of proteins from the nucleus. *Cell*. 82:463-473.

West, A.M., S.C. Rosenberg, S.N. Ur, M.K. Lehmer, Q. Ye, G. Hagemann, I. Caballero, I. Uson, A.J. MacQueen, F. Herzog, and K.D. Corbett. 2019. A conserved filamentous assembly underlies the structure of the meiotic chromosome axis. *Elife*. 8:e40372.

West, A.M.V., E.A. Komives, and K.D. Corbett. 2018. Conformational dynamics of the Hop1 HORMA domain reveal a common mechanism with the spindle checkpoint protein Mad2. *Nucleic Acids Res*. 46:279-292.

Wojtasz, L., K. Daniel, I. Roig, E. Bolcun-Filas, H. Xu, V. Boonsanay, C.R. Eckmann, H.J. Cooke, M. Jasin, S. Keeney, M.J. McKay, and A. Toth. 2009. Mouse HORMAD1 and HORMAD2, two conserved meiotic chromosomal proteins, are depleted from synapsed chromosome axes with the help of TRIP13 AAA-ATPase. *PLoS Genet*. 5:e1000702.

Yang, C., B. Hu, S.M. Portheine, P. Chuenban, and A. Schnittger. 2020. State changes of the HORMA protein ASY1 are mediated by an interplay between its closure motif and PCH2. *Nucleic Acids Res*. 48:11521-11535.

Ye, Q., D.H. Kim, I. Dereli, S.C. Rosenberg, G. Hagemann, F. Herzog, A. Toth, D.W. Cleveland, and K.D. Corbett. 2017. The AAA+ ATPase TRIP13 remodels HORMA domains through N-terminal engagement and unfolding. *EMBO J*. 36:2419-2434.

Ye, Q., S.C. Rosenberg, A. Moeller, J.A. Speir, T.Y. Su, and K.D. Corbett. 2015. TRIP13 is a protein-remodeling AAA+ ATPase that catalyzes MAD2 conformation switching. *Elife*. 4:e07367.

Zanders, S., and E. Alani. 2009. The pch2Delta mutation in baker's yeast alters meiotic crossover levels and confers a defect in crossover interference. *PLoS Genet*. 5:e1000571.

Ziolkowska, N.E., L. Karotki, M. Rehman, J.T. Huiskonen, and T.C. Walther. 2011. Eisosome-driven plasma membrane organization is mediated by BAR domains. *Nat Struct Mol Biol*. 18:854-856.

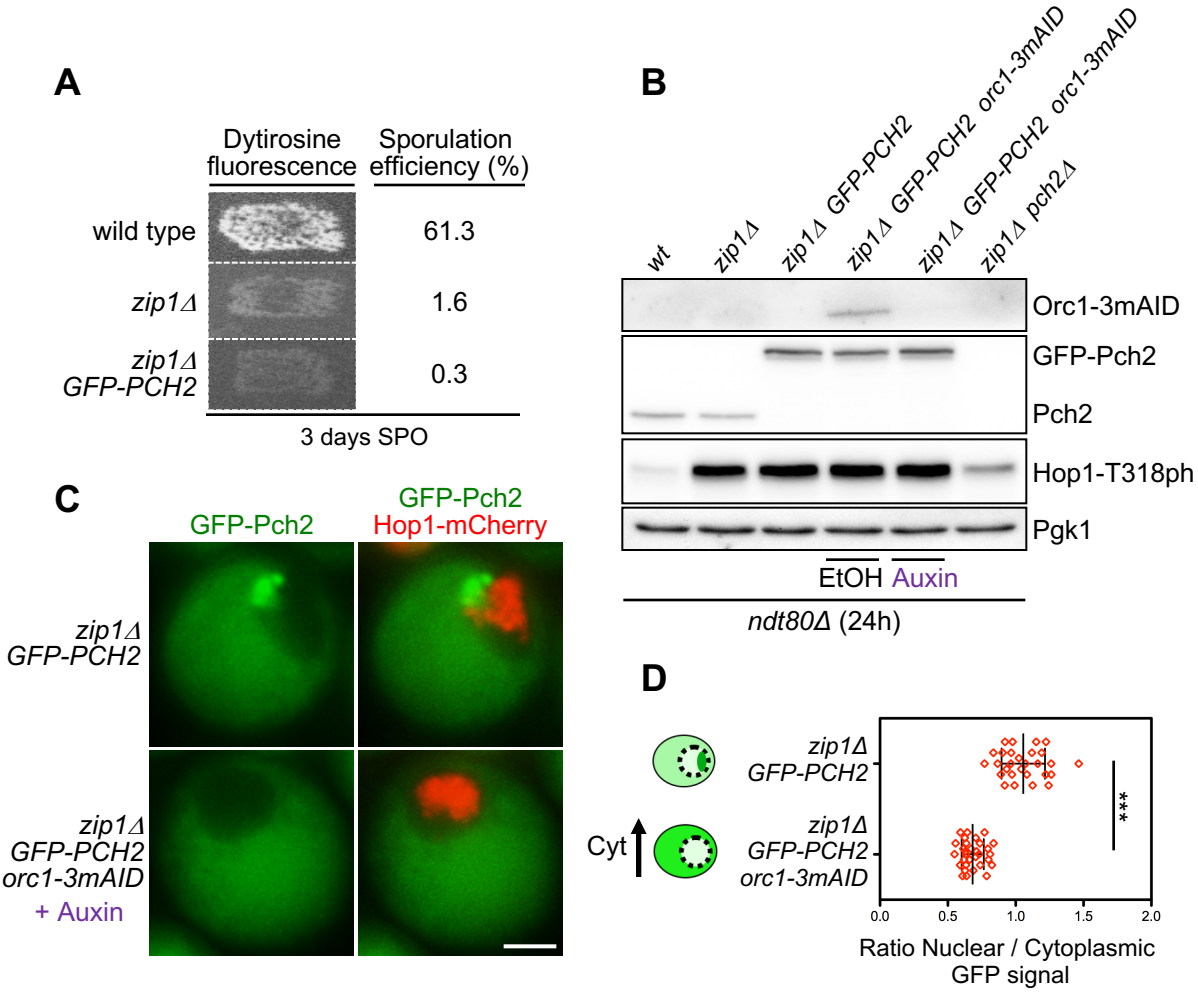
A
Dytirosine fluorescence
Sporulation efficiency (%)
wild type
61.3
zip1Δ
1.6
zip1Δ GFP-PCH2
0.3
3 days SPO
B
wt
zip1Δ
zip1Δ GFP-PCH2
zip1Δ GFP-PCH2 orc1-3mAID
zip1Δ GFP-PCH2 orc1-3mAID
zip1Δ pch2Δ
Orc1-3mAID
GFP-Pch2
Pch2
Hop1-T318ph
Pgk1
EtOH
Auxin
ndt80Δ (24h)
C
GFP-Pch2
GFP-Pch2
Hop1-mCherry
zip1Δ GFP-PCH2
zip1Δ GFP-PCH2 orc1-3mAID
+ Auxin
D
Cyt
zip1Δ GFP-PCH2
zip1Δ GFP-PCH2 orc1-3mAID
***
0.0
0.5
1.0
1.5
2.0
Ratio Nuclear / Cytoplasmic GFP signal

Figure 1

Figure 1. Cytoplasmic accumulation of Pch2 upon Orc1 depletion supports checkpoint activity.

(A) Functional analysis of the GFP-tagged version of *PCH2.* Dityrosine fluorescence, as a visual indicator of sporulation, and sporulation efficiency were examined after 3 days on sporulation plates. Strains are DP421 (wild type), DP422 (*zip1Δ*) and DP1621 (*zip1Δ GFP-PCH2)*. (**B)** Western blot analysis of Orc1-3mAID production (detected with an anti-mAID antibody), GFP-Pch2 and Pch2 production (detected with an anti-Pch2 antibody), and Hop1-T318 phosphorylation. Pgk1 was used as loading control. Strains are DP424 (*ndt80Δ*), DP428 (*ndt80Δ zip1Δ*), DP1640 (*ndt80Δ zip1Δ GFP-PCH2*), DP1630 (*ndt80Δ zip1Δ orc1-3mAID GFP-PCH2*) and DP881 (*ndt80Δ zip1Δ pch2Δ*). EtOH or auxin (500 μM) was added to *orc1-3mAID* cultures at 12 h. Samples were collected at 24 h after meiotic induction. (**C)** Fluorescence microscopy analysis of GFP-Pch2 (green) and Hop1-mCherry (red) distribution in whole meiotic cells 16 h after meiotic induction. Representative cells are shown. Scale bar, 2 μm. (**D)** Quantification of the ratio between the nuclear (including the nucleolar) and cytoplasmic GFP fluorescent signal. Error bars: SD. The cartoon illustrates the subcellular localization of GFP-Pch2 (green) in the different conditions. The strains in (C) and (D) are DP1636 (*zip1Δ GFP-PCH2*) and DP1633 (*zip1Δ orc1-3mAID GFP-PCH2*). Auxin (500 μM) was added to the *orc1-3mAID* culture 12 hours after meiotic induction.

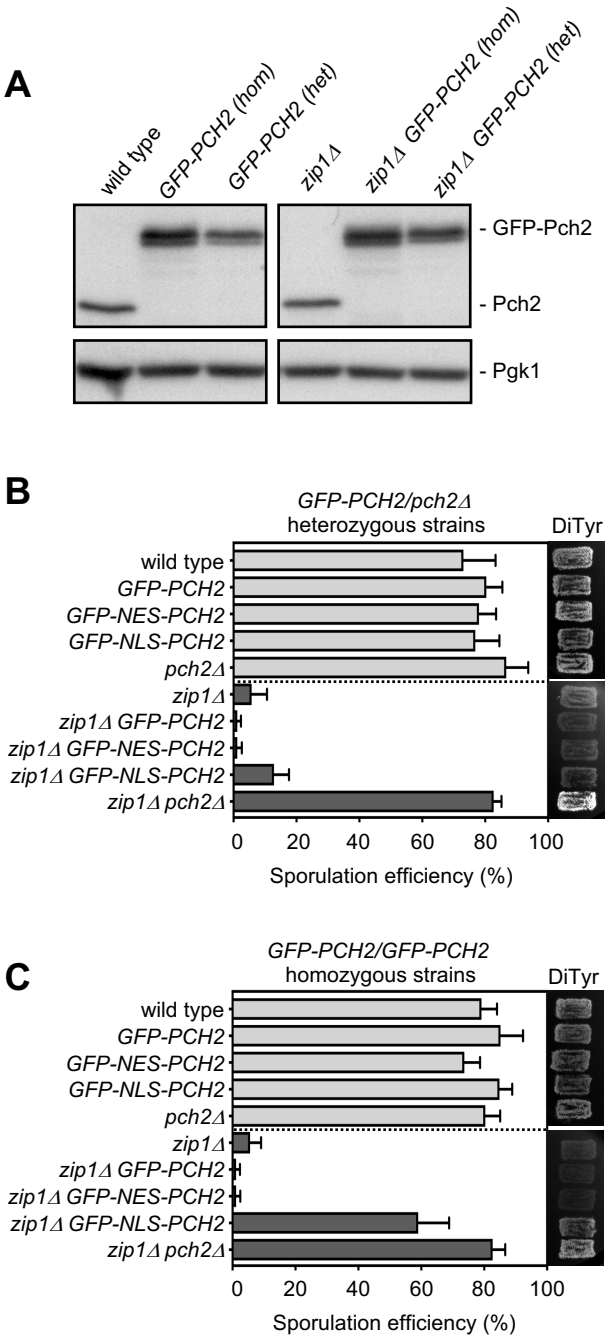
A
wild type
GFP-PCH2 (hom)
GFP-PCH2 (het)
zip1Δ
zip1Δ GFP-PCH2 (hom)
zip1Δ GFP-PCH2 (het)
- GFP-Pch2
- Pch2
- Pgk1
B
GFP-PCH2/pch2Δ
heterozygous strains
DiTyr
wild type
GFP-PCH2
GFP-NES-PCH2
GFP-NLS-PCH2
pch2Δ
zip1Δ
zip1Δ GFP-PCH2
zip1Δ GFP-NES-PCH2
zip1Δ GFP-NLS-PCH2
zip1Δ pch2Δ
0 20 40 60 80 100
Sporulation efficiency (%)
C
GFP-PCH2/GFP-PCH2
homozygous strains
DiTyr
wild type
GFP-PCH2
GFP-NES-PCH2
GFP-NLS-PCH2
pch2Δ
zip1Δ
zip1Δ GFP-PCH2
zip1Δ GFP-NES-PCH2
zip1Δ GFP-NLS-PCH2
zip1Δ pch2Δ
0 20 40 60 80 100
Sporulation efficiency (%)

Figure 2

Figure 2. Analysis of diploid strains harboring the different versions of *GFP-PCH2* integrated at its genomic locus in heterozygosis and homozygosis.

(A) Western blot analysis of GFP-Pch2 and Pch2, detected with an anti-Pch2 antibody. Pgk1 was used as loading control. Heterozygous strains are *GFP-PCH2/pch2Δ*. Strains are DP421 (wild type), DP1620 (*GFP-PCH2[hom]*), DP1624 (*GFP-PCH2[het]*), DP422 (*zip1Δ*), DP1621 (*zip1Δ GFP-PCH2[hom]*) and DP1625 (*zip1Δ GFP-PCH2[het]*). **(B, C)** Sporulation efficiency, assessed by microscopic counting of asci, and dityrosine fluorescence (DiTyr), as a visual indicator of sporulation, were examined after 3 days on sporulation plates. Error bars, SD; n=3. At least 300 cells were counted for each strain. Light grey and dark grey bars correspond to *ZIP1* and *zip1Δ* strains, respectively. Strains in (B) are: DP421 (wild type), DP1624 (*GFP-PCH2*), DP1685 (*GFP-NES-PCH2*), DP1699 (*GFP-NLS-PCH2*), DP1023 (*pch2Δ*), DP422 (*zip1Δ*), DP1625 (*zip1Δ GFP-PCH2*), DP1686 (*zip1Δ GFP-NES-PCH2*), DP1701 (*zip1Δ GFP-NLS-PCH2*), and DP1029 (*zip1Δ pch2Δ*). Strains in (C) are: DP421 (wild type), DP1620 (*GFP-PCH2*), DP1669 (*GFP-NES-PCH2*), DP1695 (*GFP-NLS-PCH2*), DP1023 (*pch2Δ*), DP422 (*zip1Δ*), DP1621(*zip1Δ GFP-PCH2*), DP1670 (*zip1Δ GFP-NES-PCH2*), DP1696 (*zip1Δ GFP-NLS-PCH2*), and DP1029 (*zip1Δ pch2Δ*).

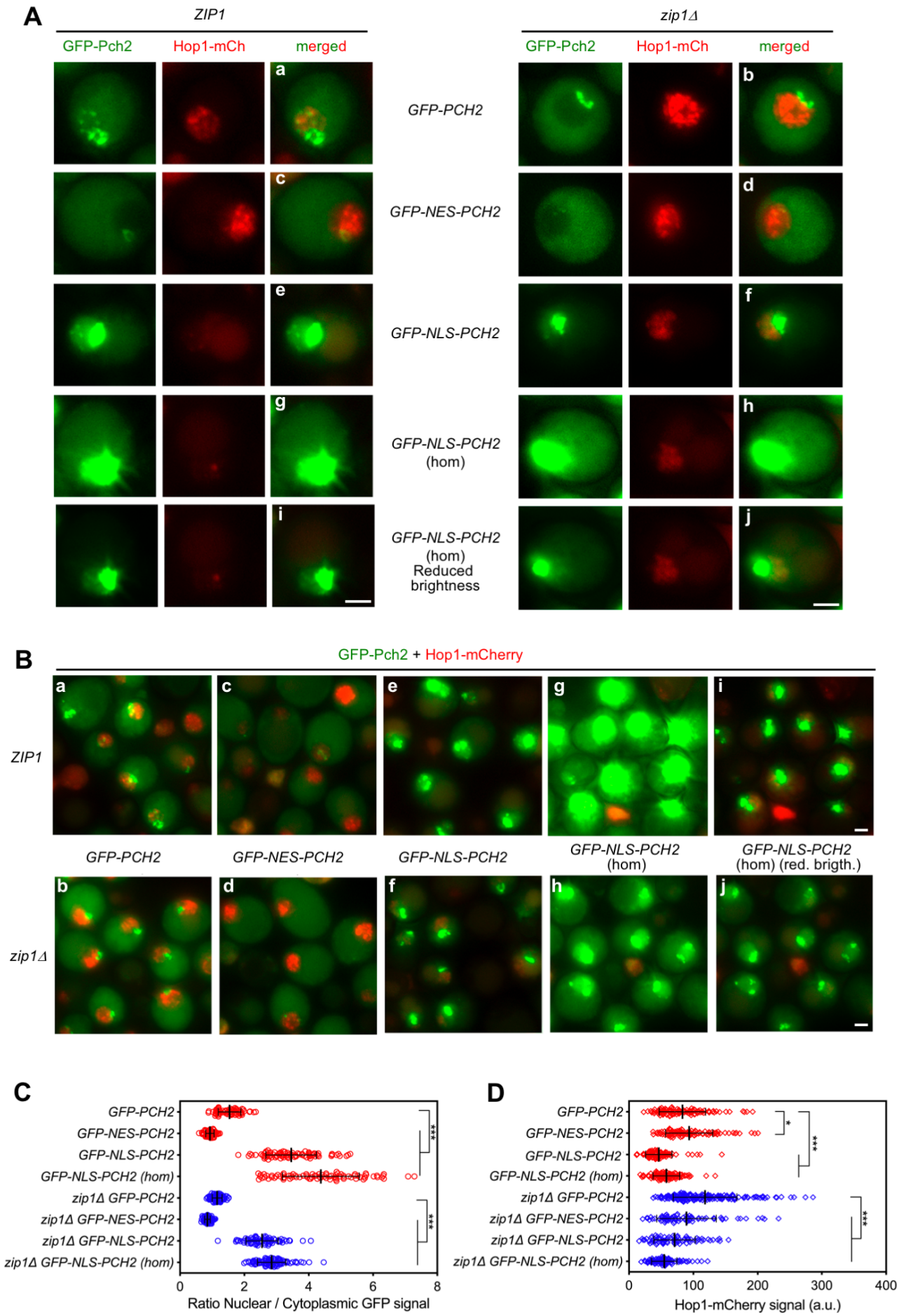
A
ZIP1
zip1Δ
GFP-Pch2
Hop1-mCh
merged
GFP-PCH2
GFP-NES-PCH2
GFP-NLS-PCH2
GFP-NLS-PCH2 (hom)
GFP-NLS-PCH2 (hom) Reduced brightness
a
b
c
d
e
f
g
h
i
j
B
GFP-Pch2 + Hop1-mCherry
ZIP1
zip1Δ
GFP-PCH2
GFP-NES-PCH2
GFP-NLS-PCH2
GFP-NLS-PCH2 (hom)
GFP-NLS-PCH2 (hom) (red. brigth.)
C
GFP-PCH2
GFP-NES-PCH2
GFP-NLS-PCH2
GFP-NLS-PCH2 (hom)
zip1Δ GFP-PCH2
zip1Δ GFP-NES-PCH2
zip1Δ GFP-NLS-PCH2
zip1Δ GFP-NLS-PCH2 (hom)
***
0
2
4
6
8
Ratio Nuclear / Cytoplasmic GFP signal
D
*
***
0
100
200
300
400
Hop1-mCherry signal (a.u.)

Figure 3

Figure 3. Subcellular localization of GFP-NES-Pch2 and GFP-NLS-Pch2.

(A, B) Fluorescence microscopy analysis of genomic-expressed GFP-Pch2, GFP-NES-Pch2 or GFP-NLS-Pch2 (green) and Hop1-mCherry (red) localization in *ZIP1* and *zip1Δ* whole meiotic cells 16 h after meiotic induction. Representative individual cells and representative fields are shown in (A) and (B), respectively. All images were acquired and processed with similar settings, but in the case of *GFP-NLS-PCH2* homozygous *(hom)* cells, additional panels (i, j) with reduced GFP brightness are presented for better visualization of the strong original signal. Scale bar, 2 μm. **(C)** Quantification of the ratio of nuclear (including nucleolar) to cytoplasmic GFP fluorescent signal. Error bars: SD. **(D)** Quantification of the Hop1-mCherry fluorescent signal. Error bars: SD; a.u., arbitrary units. In (C) and (D), red and blue symbols correspond to *ZIP1* and *zip1Δ* strains, respectively. Strains are: DP1650 (*GFP-PCH2*), DP1687 (*GFP-NES-PCH2*), DP1700 (*GFP-NLS-PCH2*), DP1697 (*GFP-NLS-PCH2[hom]*), DP1651 (*zip1Δ GFP-PCH2*), DP1688 (*zip1Δ GFP-NES-PCH2*), DP1702 (*zip1Δ GFP-NLS-PCH2*), and DP1698 (*zip1Δ GFP-NLS-PCH2[hom]*).

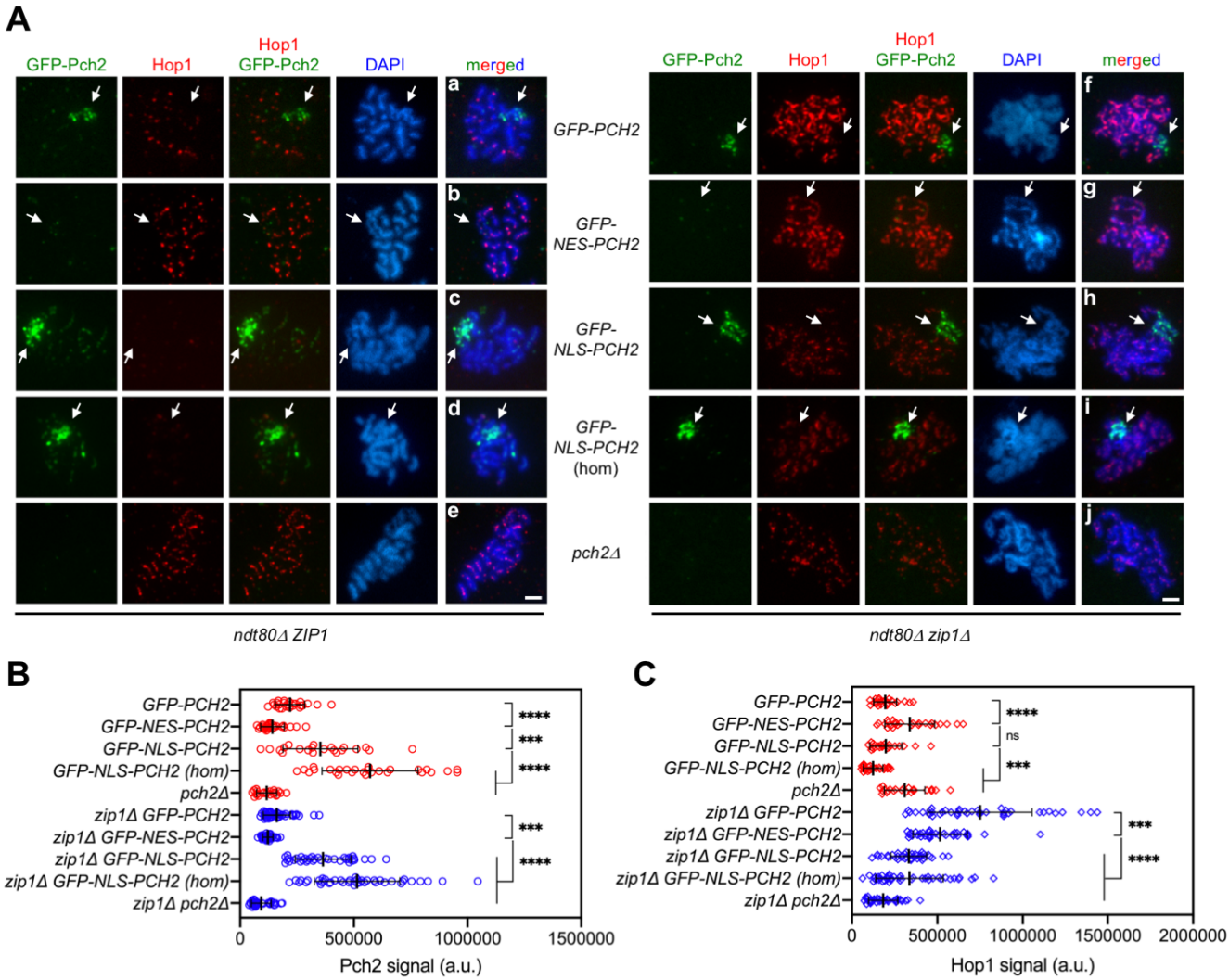
A
GFP-Pch2
Hop1
Hop1
GFP-Pch2
DAPI
merged
GFP-PCH2
GFP-NES-PCH2
GFP-NLS-PCH2
GFP-NLS-PCH2 (hom)
pch2Δ
ndt80Δ ZIP1
ndt80Δ zip1Δ
B
GFP-PCH2
GFP-NES-PCH2
GFP-NLS-PCH2
GFP-NLS-PCH2 (hom)
pch2Δ
zip1Δ GFP-PCH2
zip1Δ GFP-NES-PCH2
zip1Δ GFP-NLS-PCH2
zip1Δ GFP-NLS-PCH2 (hom)
zip1Δ pch2Δ
Pch2 signal (a.u.)
C
Hop1 signal (a.u.)
ns

Figure 4

Figure 4. Impact of GFP-NES-Pch2 and GFP-NLS-Pch2 on the pattern of Hop1 chromosomal localization.

(A) Immunofluorescence of meiotic chromosomes stained with anti-GFP antibodies (to detect GFP-Pch2; green), anti-Hop1 antibodies (red) and DAPI (blue). Representative *ZIP1* and *zip1Δ* nuclei, as indicated, are shown. Arrows point to the rDNA region. Spreads were prepared from *ndt80Δ* strains at 24 h. Scale bar, 2 µm. **(B, C)** Quantification of the GFP-Pch2 and Hop1 signal, respectively. Error bars: SD; a.u., arbitrary units. Red and blue symbols correspond to *ZIP1* and *zip1Δ* strains, respectively. Strains are: DP1654 (*GFP-PCH2*), DP1725 (*GFP-NES-PCH2*), DP1729 (*GFP-NLS-PCH2*), DP1768 (*GFP-NLS-PCH2 [hom]*), DP1058 (*pch2Δ*), DP1655 (*zip1Δ GFP-PCH2*), DP1726 (*zip1Δ GFP-NES-PCH2*), DP1730 (*zip1Δ GFP-NLS-PCH2*), DP1769 (*zip1Δ GFP-NLS-PCH2 [hom]*) and DP881 (*zip1Δ pch2Δ*).

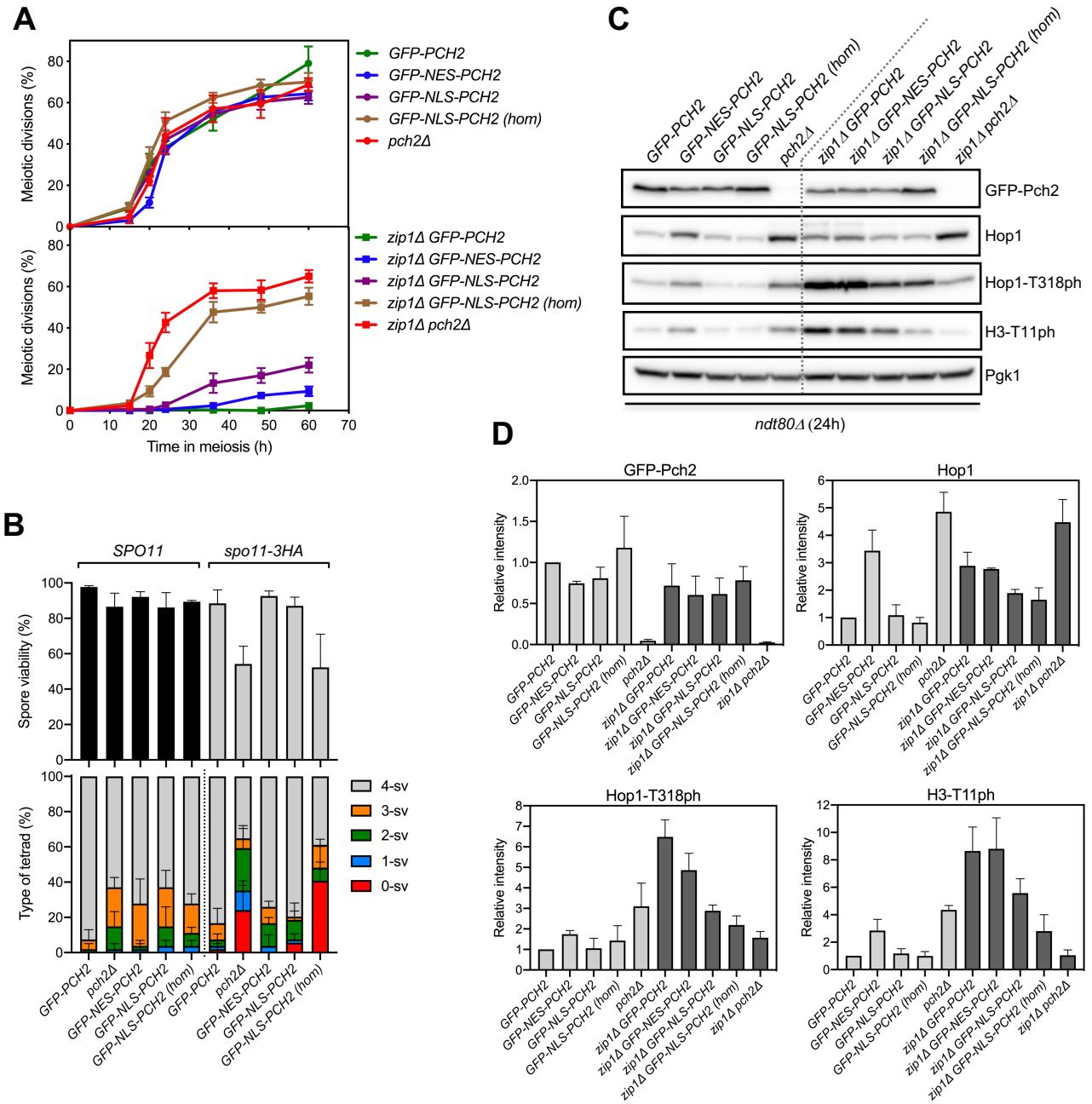
A
Meiotic divisions (%)
GFP-PCH2
GFP-NES-PCH2
GFP-NLS-PCH2
GFP-NLS-PCH2 (hom)
pch2Δ
zip1Δ GFP-PCH2
zip1Δ GFP-NES-PCH2
zip1Δ GFP-NLS-PCH2
zip1Δ GFP-NLS-PCH2 (hom)
zip1Δ pch2Δ
Time in meiosis (h)
B
SPO11
spo11-3HA
Spore viability (%)
Type of tetrad (%)
4-sv
3-sv
2-sv
1-sv
0-sv
C
GFP-PCH2
GFP-NES-PCH2
GFP-NLS-PCH2
GFP-NLS-PCH2 (hom)
pch2Δ
zip1Δ GFP-PCH2
zip1Δ GFP-NES-PCH2
zip1Δ GFP-NLS-PCH2
zip1Δ GFP-NLS-PCH2 (hom)
zip1Δ pch2Δ
GFP-Pch2
Hop1
Hop1-T318ph
H3-T11ph
Pgk1
ndt80Δ (24h)
D
GFP-Pch2
Hop1
Hop1-T318ph
H3-T11ph
Relative intensity

Figure 5

Figure 5. The largely cytoplasmic GFP-NES-Pch2 version supports checkpoint function. **(A)** Time course analysis of meiotic nuclear divisions; the percentage of cells containing two or more nuclei is represented. Error bars: SD; n=3. At least 300 cells were scored for each strain at every time point. **(B)** Spore viability assessed by tetrad dissection is shown in the top graph. The percentage of tetrads containing 4-, 3-, 2-, 1-, and 0-viable spores is presented in the bottom graph. At least 54 tetrads were dissected for each strain. Error bars, SD; n=3. **(C)** Representative western blot analysis of GFP-Pch2 and Hop1 production, and Hop1-T318 and H3-T11 phosphorylation (ph), in *ndt80Δ*-arrested strains of the indicated genotypes. Cell extracts were prepared at 24 hours in meiosis. (**D)** Quantification of GFP-Pch2, Hop1, Hop1-T318ph and H3-T11ph relative levels analyzed as in (C). The intensity values for each protein in each strain were normalized to Pgk1 and relativized to those of the wild-type *GFP-PCH2* strain. Error bars, SD; n=3. Light grey and dark grey bars correspond to *ZIP1* and *zip1Δ* strains, respectively. Strains in (**A**) are: DP1624 (*GFP-PCH2*), DP1685 (*GFP-NES-PCH2*), DP1699 (*GFP-NLS-PCH2*), DP1695 (*GFP-NLS-PCH2 [hom]*), DP1023 (*pch2Δ*), DP1625 (*zip1Δ GFP-PCH2*), DP1686 (*zip1Δ GFP-NES-PCH2*), DP1701 (*zip1Δ GFP-NLS-PCH2*), DP1696 (*zip1Δ GFP-NLS-PCH2 [hom]*) and DP1029 (*zip1Δ pch2Δ*). Strains in (B) are: DP1624 (*GFP-PCH2*), DP1023 (*pch2Δ*), DP1685 (*GFP-NES-PCH2*), DP1699 (*GFP-NLS-PCH2*), DP1695 (*GFP-NLS-PCH2 [hom]*), DP1789 (*spo11-3HA GFP-PCH2*), DP1787 (*spo11-3HA pch2Δ*), DP1791 (*spo11-3HA GFP-NES-PCH2*), DP1793 (*spo11-3HA GFP-NLS-PCH2*) and DP1792 (*spo11-3HA GFP-NLS-PCH2 [hom]*). Strains in (C, D) are: DP1654 (*ndt80Δ GFP-PCH2*), DP1725 (*ndt80Δ GFP-NES-PCH2*), DP1729 (*ndt80Δ GFP-NLS-PCH2*), DP1768 (*ndt80Δ GFP-NLS-PCH2 [hom]*), DP1058 (*ndt80Δ pch2Δ*), DP1655 (*ndt80Δ zip1Δ GFP-PCH2*), DP1726 (*ndt80Δ zip1Δ GFP-NES-PCH2*), DP1730 (*ndt80Δ zip1Δ GFP-NLS-PCH2*), DP1769 (*ndt80Δ zip1Δ GFP-NLS-PCH2 [hom]*) and DP881 (*ndt80Δ zip1Δ pch2Δ*).

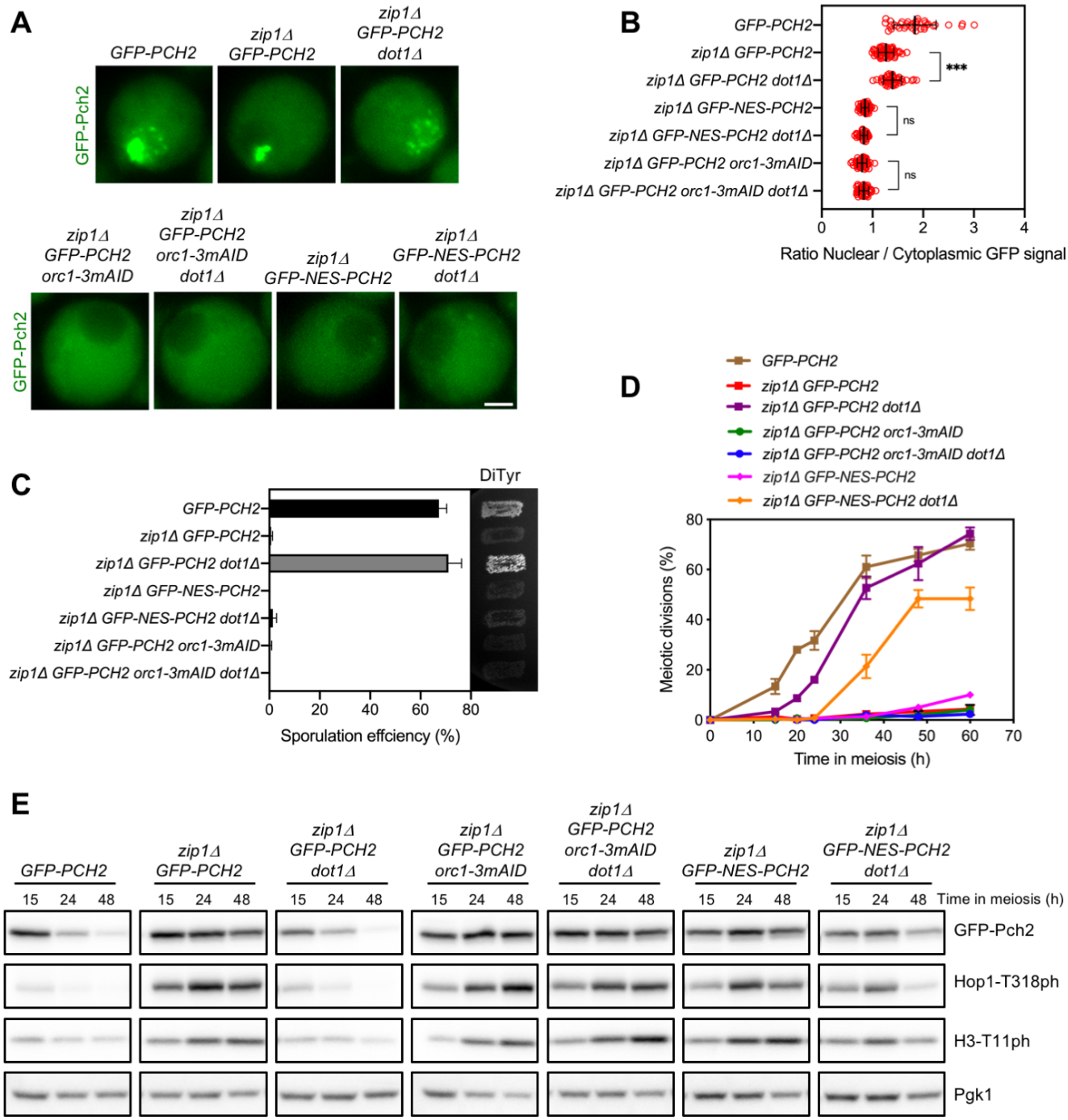
A
GFP-PCH2
zip1Δ GFP-PCH2
zip1Δ GFP-PCH2 dot1Δ
GFP-Pch2
zip1Δ GFP-PCH2 orc1-3mAID
zip1Δ GFP-PCH2 orc1-3mAID dot1Δ
zip1Δ GFP-NES-PCH2
zip1Δ GFP-NES-PCH2 dot1Δ
B
GFP-PCH2
zip1Δ GFP-PCH2
zip1Δ GFP-PCH2 dot1Δ
zip1Δ GFP-NES-PCH2
zip1Δ GFP-NES-PCH2 dot1Δ
zip1Δ GFP-PCH2 orc1-3mAID
zip1Δ GFP-PCH2 orc1-3mAID dot1Δ
***
ns
ns
0 1 2 3 4
Ratio Nuclear / Cytoplasmic GFP signal
C
DiTyr
GFP-PCH2
zip1Δ GFP-PCH2
zip1Δ GFP-PCH2 dot1Δ
zip1Δ GFP-NES-PCH2
zip1Δ GFP-NES-PCH2 dot1Δ
zip1Δ GFP-PCH2 orc1-3mAID
zip1Δ GFP-PCH2 orc1-3mAID dot1Δ
0 20 40 60 80
Sporulation effciency (%)
D
GFP-PCH2
zip1Δ GFP-PCH2
zip1Δ GFP-PCH2 dot1Δ
zip1Δ GFP-PCH2 orc1-3mAID
zip1Δ GFP-PCH2 orc1-3mAID dot1Δ
zip1Δ GFP-NES-PCH2
zip1Δ GFP-NES-PCH2 dot1Δ
Meiotic divisions (%)
0 20 40 60 80
0 10 20 30 40 50 60 70
Time in meiosis (h)
E
GFP-PCH2
zip1Δ GFP-PCH2
zip1Δ GFP-PCH2 dot1Δ
zip1Δ GFP-PCH2 orc1-3mAID
zip1Δ GFP-PCH2 orc1-3mAID dot1Δ
zip1Δ GFP-NES-PCH2
zip1Δ GFP-NES-PCH2 dot1Δ
15 24 48
Time in meiosis (h)
GFP-Pch2
Hop1-T318ph
H3-T11ph
Pgk1

Figure 6

Figure 6. Dot1 is exclusively required for Pch2 nucleolar confinement.

(A) Fluorescence microscopy analysis of GFP-Pch2 distribution in whole meiotic cells of the indicated genotypes 15 hours after meiotic induction. Representative cells are shown. Scale bar, 2 µm. **(B)** Quantification of the ratio of nuclear (including nucleolar) to cytoplasmic GFP fluorescent signal in cells analyzed as in (A). Error bars: SD. **(C)** Sporulation efficiency, assessed by microscopic counting of asci, and dityrosine fluorescence (DiTyr), as a visual indicator of sporulation, were examined after 3 days on sporulation plates. Error bars, SD; n=3. At least 300 cells were counted for each strain. **(D)** Time course analysis of meiotic nuclear divisions; the percentage of cells containing two or more nuclei is represented. Error bars: SD; n=3. At least 300 cells were scored for each strain at every time point. **(E)** Western blot analysis of GFP-Pch2 production, and Hop1-T318 and H3-T11 phosphorylation (ph), at different meiotic time points. Pgk1 was used as a loading control. In all experiments, auxin (500 µM) was added 12 hours after meiotic induction to induce Orc1-3mAID depletion in cells harboring the degron allele (Herruzo et al., 2019). Strains in (A-E) are: DP1624 (*GFP-PCH2*), DP1625 (*zip1Δ GFP- PCH2*), DP1734 (*zip1Δ GFP-PCH2 dot1Δ*), DP1644 (*zip1Δ GFP-PCH2 orc1-3mAID*), DP1746 (*zip1Δ GFP-PCH2 orc1-3mAID dot1Δ*), DP1686 (*zip1Δ GFP-NES-PCH2*) and DP1747 (*zip1Δ GFP-NES-PCH2 dot1Δ*).

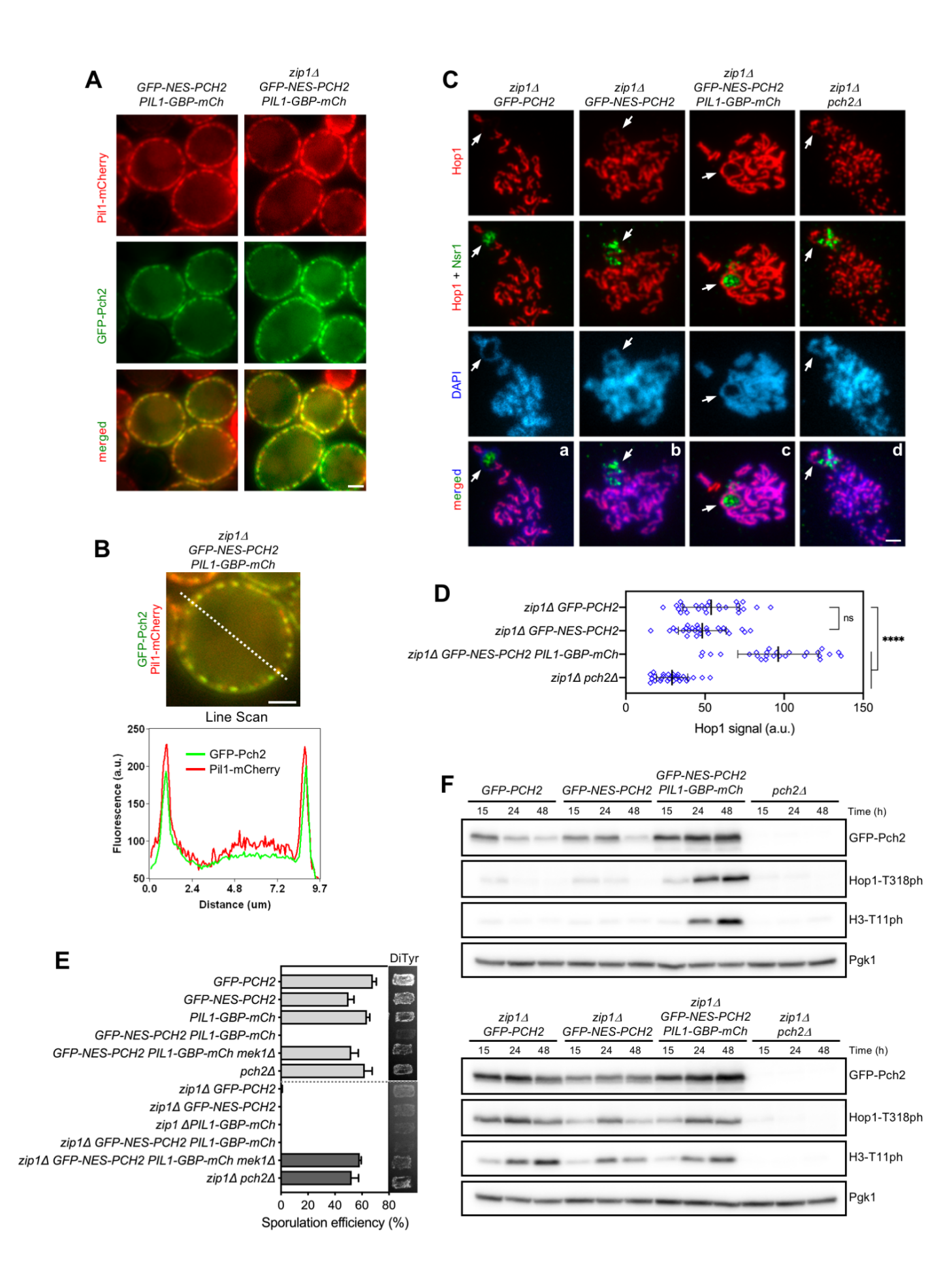
A
GFP-NES-PCH2
PIL1-GBP-mCh
zip1Δ
GFP-NES-PCH2
PIL1-GBP-mCh
Pil1-mCherry
GFP-Pch2
merged
B
zip1Δ
GFP-NES-PCH2
PIL1-GBP-mCh
GFP-Pch2
Pil1-mCherry
Line Scan
GFP-Pch2
Pil1-mCherry
Fluorescence (a.u.)
Distance (um)
C
zip1Δ
GFP-PCH2
zip1Δ
GFP-NES-PCH2
zip1Δ
GFP-NES-PCH2
PIL1-GBP-mCh
zip1Δ
pch2Δ
Hop1
Hop1 + Nsr1
DAPI
merged
a
b
c
d
D
zip1Δ GFP-PCH2
zip1Δ GFP-NES-PCH2
zip1Δ GFP-NES-PCH2 PIL1-GBP-mCh
zip1Δ pch2Δ
ns
****
Hop1 signal (a.u.)
E
DiTyr
GFP-PCH2
GFP-NES-PCH2
PIL1-GBP-mCh
GFP-NES-PCH2 PIL1-GBP-mCh
GFP-NES-PCH2 PIL1-GBP-mCh mek1Δ
pch2Δ
zip1Δ GFP-PCH2
zip1Δ GFP-NES-PCH2
zip1 ΔPIL1-GBP-mCh
zip1Δ GFP-NES-PCH2 PIL1-GBP-mCh
zip1Δ GFP-NES-PCH2 PIL1-GBP-mCh mek1Δ
zip1Δ pch2Δ
Sporulation efficiency (%)
F
GFP-PCH2
GFP-NES-PCH2
GFP-NES-PCH2
PIL1-GBP-mCh
pch2Δ
Time (h)
GFP-Pch2
Hop1-T318ph
H3-T11ph
Pgk1
zip1Δ
GFP-PCH2
zip1Δ
GFP-NES-PCH2
zip1Δ
GFP-NES-PCH2
PIL1-GBP-mCh
zip1Δ
pch2Δ
Time (h)
GFP-Pch2
Hop1-T318ph
H3-T11ph
Pgk1

Figure 7

Figure 7. Immobilization of Pch2 at the cell periphery leads to constitutive checkpoint induction.

(A) Fluorescence microscopy analysis of GFP-Pch2 and Pil1-GBP-mCherry distribution in whole meiotic cells of the indicated genotypes 16 hours after meiotic induction. Scale bar, 2 μm. **(B)** A representative cell and the corresponding Line Scan plot are shown to highlight GFP-Pch2 and Pil1-GBP-mCherry colocalization. The graph represents the GFP and mCherry fluorescent signals (green and red, respectively) along the depicted dotted line from left to right (a.u., arbitrary units). Scale bar, 2 μm. **(C)** Immunofluorescence of meiotic chromosomes stained with anti-Hop1 (red) and anti-Nsr1 (nucleolar marker; green) antibodies, and DAPI (blue). Arrows point to the rDNA region. Spreads were prepared at 16 h. Scale bar, 2 μm. **(D)** Quantification of the Hop1 signal on spreads. Error bars: SD; a.u., arbitrary units. **(E)** Sporulation efficiency and dityrosine fluorescence (DiTyr) were examined after 3 days on sporulation plates. Error bars, SD; n=3. At least 300 cells were counted for each strain. **(F)** Western blot analysis of GFP-Pch2 production and checkpoint activation markers (Hop1-T318 and H3-T11 phosphorylation), at different meiotic time points. Pgk1 was used as a loading control. Strains in (A-E) are: DP1624 (*GFP-PCH2*), DP1685 (*GFP-NES-PCH2*), DP1802 (*PIL1-GBP-mCherry*), DP1795 (*GFP-NES-PCH2 PIL1-GBP-mCherry*), DP1811 (*GFP-NES-PCH2 PIL1-GBP-mCherry mek1Δ*), DP1023 (*pch2Δ*), DP1625 (*zip1Δ GFP-PCH2*), DP1686 (*zip1Δ GFP-NES-PCH2*), DP1803 (*zip1Δ PIL1-GBP-mCherry*), DP1796 (*zip1Δ GFP-NES-PCH2 PIL1-GBP-mCherry*), DP1812 (*zip1Δ GFP-NES-PCH2 PIL1-GBP-mCherry mek1Δ*) and DP1029 (*zip1Δ pch2Δ*).

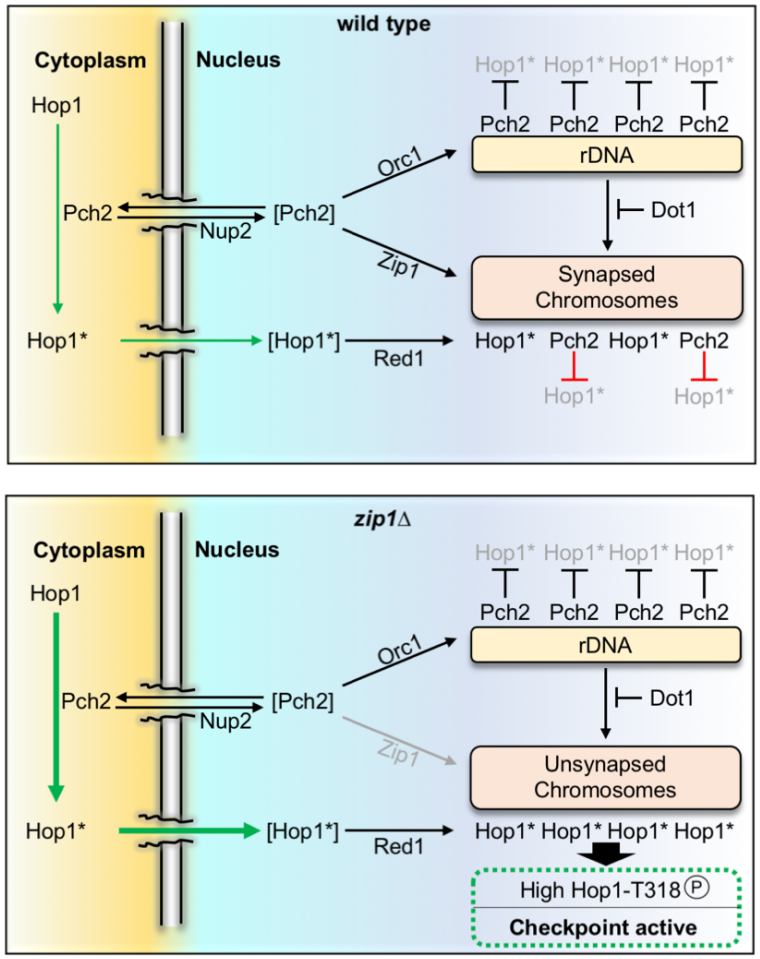
wild type
Cytoplasm
Nucleus
Hop1
Pch2
Nup2
[Pch2]
Hop1*
[Hop1*]
Red1
Orc1
Zip1
Hop1* Hop1* Hop1* Hop1*
Pch2 Pch2 Pch2 Pch2
rDNA
Dot1
Synapsed Chromosomes
Hop1* Pch2 Hop1* Pch2
Hop1* Hop1*
zip1Δ
Cytoplasm
Nucleus
Hop1
Pch2
Nup2
[Pch2]
Hop1*
[Hop1*]
Red1
Orc1
Zip1
Hop1* Hop1* Hop1* Hop1*
Pch2 Pch2 Pch2 Pch2
rDNA
Dot1
Unsynapsed Chromosomes
Hop1* Hop1* Hop1* Hop1*
High Hop1-T318 P
Checkpoint active

Figure 8

Figure 8. Model of Pch2 function in the meiotic recombination checkpoint induced by the lack of Zip1.

The population of Pch2 present in the cytoplasm acts on Hop1 to provoke a conformational change (asterisk) that poises Hop1 for its transport to the nucleus and the incorporation on chromosomes via Red1 interaction. The precise distribution of Pch2 among cytoplasm, rDNA and synapsed chromosomes is carefully balanced by the factors depicted. In the wild type, Zip1-mediated recruitment of Pch2 to synapsed chromosomes leads to Hop1 eviction likely by releasing the interaction with Red1. In the *zip1Δ* mutant, Pch2 does not localize to chromosomes and the cytoplasmic pool is increased further stimulating Hop1 incorporation on the unsynapsed axes and the subsequent Mec1-dependent phosphorylation at T318 to launch the downstream checkpoint activation response. Proteins between brackets represent transient states. See text and Figure S6 for additional details and model of action in different circumstances.

Table 1. Summary of Pch2 subcellular localization, Hop1 chromosomal distribution and checkpoint activity in different situations

	Pch2 subcellular localization				Hop1 localization		
Relevant Genotype[1]	**Chromosomes**	**Nucleolus (rDNA)**	**Cytoplasm**	**Other**	**Chromosome axes**	**Nucleolus (rDNA)**	**Checkpoint Activity**
wild type	+ (faint foci)	+	+	-	foci	-	na
zip1Δ	-	+	+	-	linear	-	+
zip1Δ pch2Δ	-	-	-	-	discontinuous	+	-
zip1Δ orc1-3mAID	-	-	+	-	linear[2]	+[2]	+
zip1Δ NES-PCH2	-	-/+	+	-	linear	+	+
zip1Δ NLS-PCH2 (het)	-	+	-/+	nucleoplasm	discontinuous	-	-/+
zip1Δ NLS-PCH2 (hom)	-	+	-/+	nucleoplasm	discontinuous	-	-
zip1Δ dot1Δ	+ (widespread)	+	+	-	discontinuous[3]	+/-[3]	-
zip1Δ orc1-3mAID dot1Δ	-	-	+	-	nd	nd	+
zip1Δ nup2Δ	-	+/-	+	-	nd	nd	+
zip1Δ PIL1-GBP	-	-	-	eisosomes	strong linear	+	+

(1) Strains carry GFP-tagged *PCH2.*
(2) Data from Herruzo et al. 2019.
(3) Data from Ontoso et al. 2013.
na: not applicable; nd: not determined.

SUPPLEMENTAL MATERIAL

Pch2 orchestrates the meiotic recombination checkpoint from the cytoplasm

Esther Herruzo[1], Ana Lago-Maciel[1], Sara Baztán[1], Beatriz Santos[1,2], Jesús A. Carballo[3] and Pedro A. San-Segundo[1,*]

[1]Instituto de Biología Funcional y Genómica (IBFG). Consejo Superior de Investigaciones Científicas (CSIC) and University of Salamanca. 37007-Salamanca, Spain

[2]Departamento de Microbiología y Genética. University of Salamanca. 37007-Salamanca, Spain.

[3]Department of Cellular and Molecular Biology. Centro de Investigaciones Biológicas Margarita Salas. Consejo Superior de Investigaciones Científicas (CSIC). 28040-Madrid, Spain

*Corresponding author: pedross@usal.es; +34 923294902

Supplemental Figures S1-S6

Supplemental Tables S1-S3

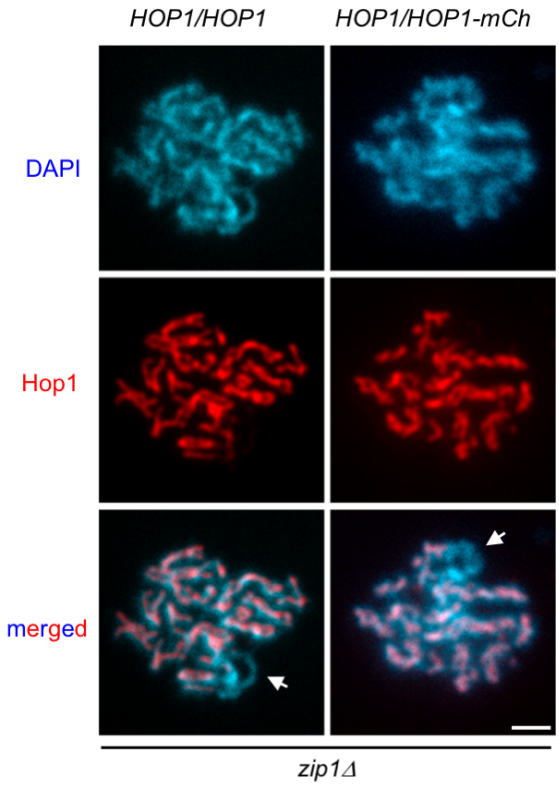

Figure S1. Hop1 axial localization is normal in *HOP1/HOP1-mCherry* strains. Immunofluorescence of meiotic chromosomes stained with anti-Hop1 (red) and DAPI (blue). Arrows point to the rDNA region devoid of Hop1. Spreads were prepared at 16 h. Scale bar, 2 µm. Strains are: DP422 (*zip1Δ HOP1/HOP1*) and DP1500 (*zip1Δ HOP1/HOP1-mCherry*).

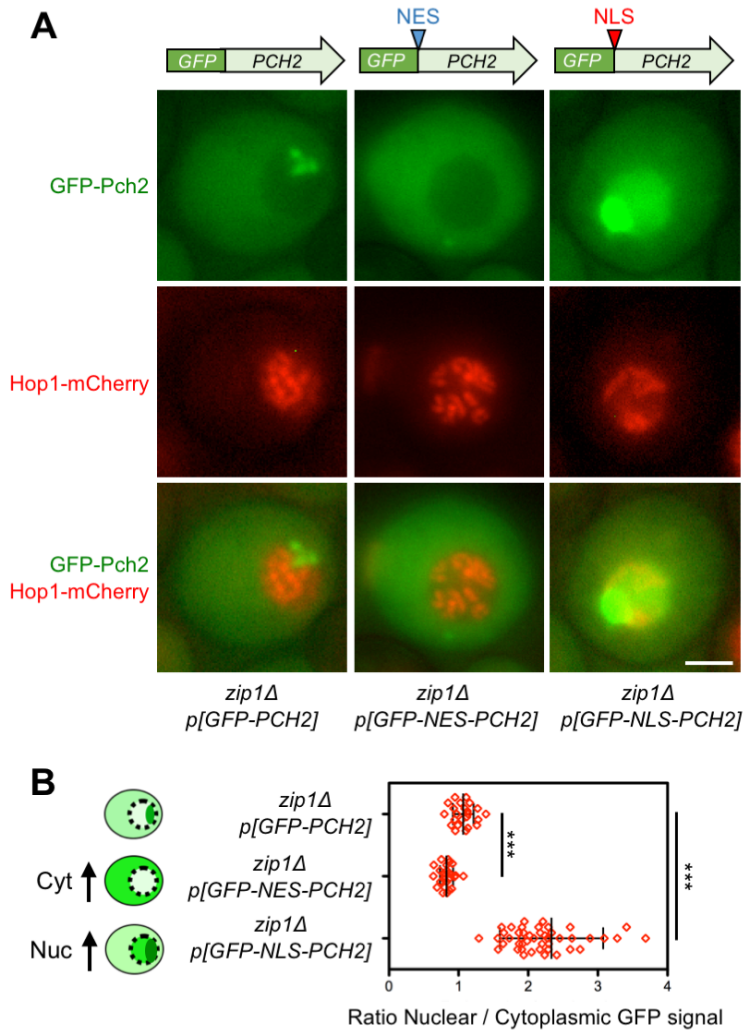

Figure S2. Redirecting Pch2 subcellular distribution by addition of NES or NLS sequences.

(A) Fluorescence microscopy analysis of plasmid-expressed GFP-Pch2, GFP-NES-Pch2 or GFP-NLS-Pch2 (green) and Hop1-mCherry (red) in whole meiotic cells 15 h after meiotic induction. Representative cells are shown. Scale bar, 2 µm. **(B)** Quantification of the ratio of nuclear (including nucleolar) to cytoplasmic GFP fluorescent signal. Error bars: SD. The cartoon illustrates the subcellular localization of the different versions of GFP-Pch2 (green). The strain in (A) and (B) is DP1500 (*zip1Δ)* transformed with the centromeric plasmids pSS393 (*GFP-PCH2),* pSS408 *(GFP-NES-PCH2)* and pSS421 (*GFP-NLS-PCH2*).

Figure S3

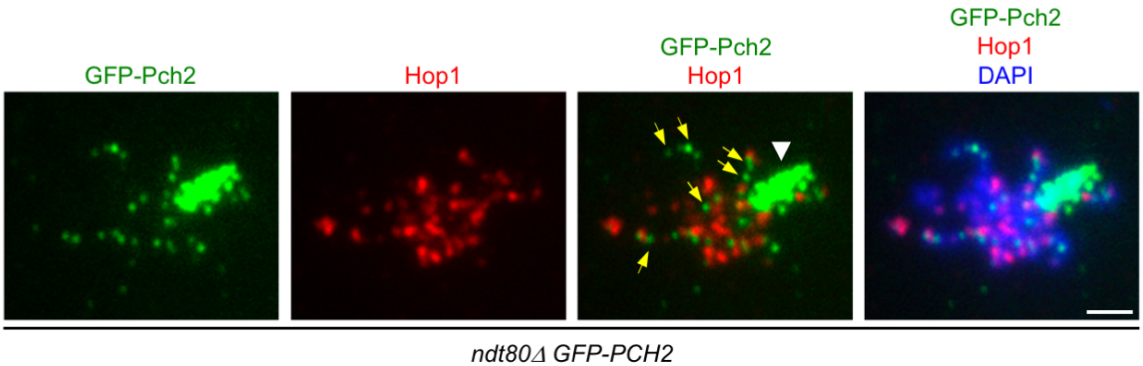

Figure S3. GFP-Pch2 localizes to foci on synapsed chromosomes alternating with Hop1.

Immunofluorescence of meiotic chromosomes stained with anti-GFP antibodies (to detect GFP-Pch2; green), anti-Hop1 antibodies (red) and DAPI (blue). White arrowhead points to the rDNA. Yellow arrows point to interstitial GFP-Pch2 foci alternating with Hop1 signal. The Pch2 signal was computer-enhanced to visualize chromosomal foci. Spreads were prepared from *ndt80Δ* strains at 24 h. Scale bar, 2 μm. The strain is DP1654.

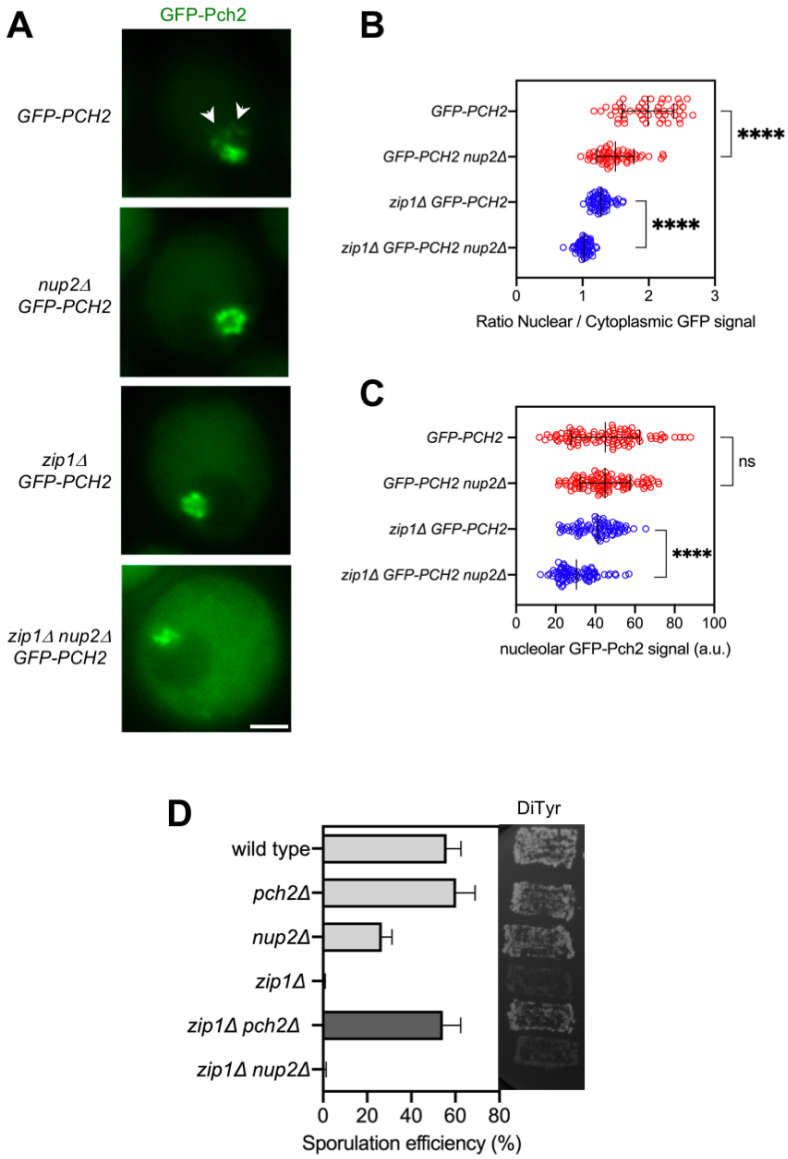

Figure S4. Nup2 regulates Pch2 subcellular localization, but it is not required for the checkpoint triggered by *zip1Δ*.

(A) Fluorescence microscopy analysis of GFP-Pch2 distribution in whole meiotic cells of the indicated genotypes 16 hours after meiotic induction. Representative cells are shown. Arrows point to chromosomal (non-nucleolar) Pch2. Scale bar, 2 µm. **(B, C)** Quantification of the ratio of nuclear (including nucleolar) to cytoplasmic GFP fluorescent signal **(B)** and the nucleolar GFP-Pch2 signal **(C)** in cells analyzed as in **(A).** Error bars: SD. **(D)** Sporulation efficiency, assessed by microscopic counting of asci, and dityrosine fluorescence (DiTyr), as a visual indicator of sporulation, were examined after 3 days on sporulation plates. Error bars, SD; n=3. At least 300 cells were counted for each strain. Strains in (A-C) are: DP1624 (*GFP-PCH2*), DP1744 (*nup2Δ GFP-PCH2*), DP1625 (*zip1Δ GFP-PCH2*) and DP1745 (*zip1Δ nup2Δ GFP-PCH2*). Strains in (D) are: DP1151 (wild type), DP1164 (*pch2Δ*), DP1723 (*nup2Δ*), DP1152 (*zip1Δ*), DP1161(*zip1Δ pch2Δ*) and DP1724 (*zip1Δ nup2Δ*).

Figure S5

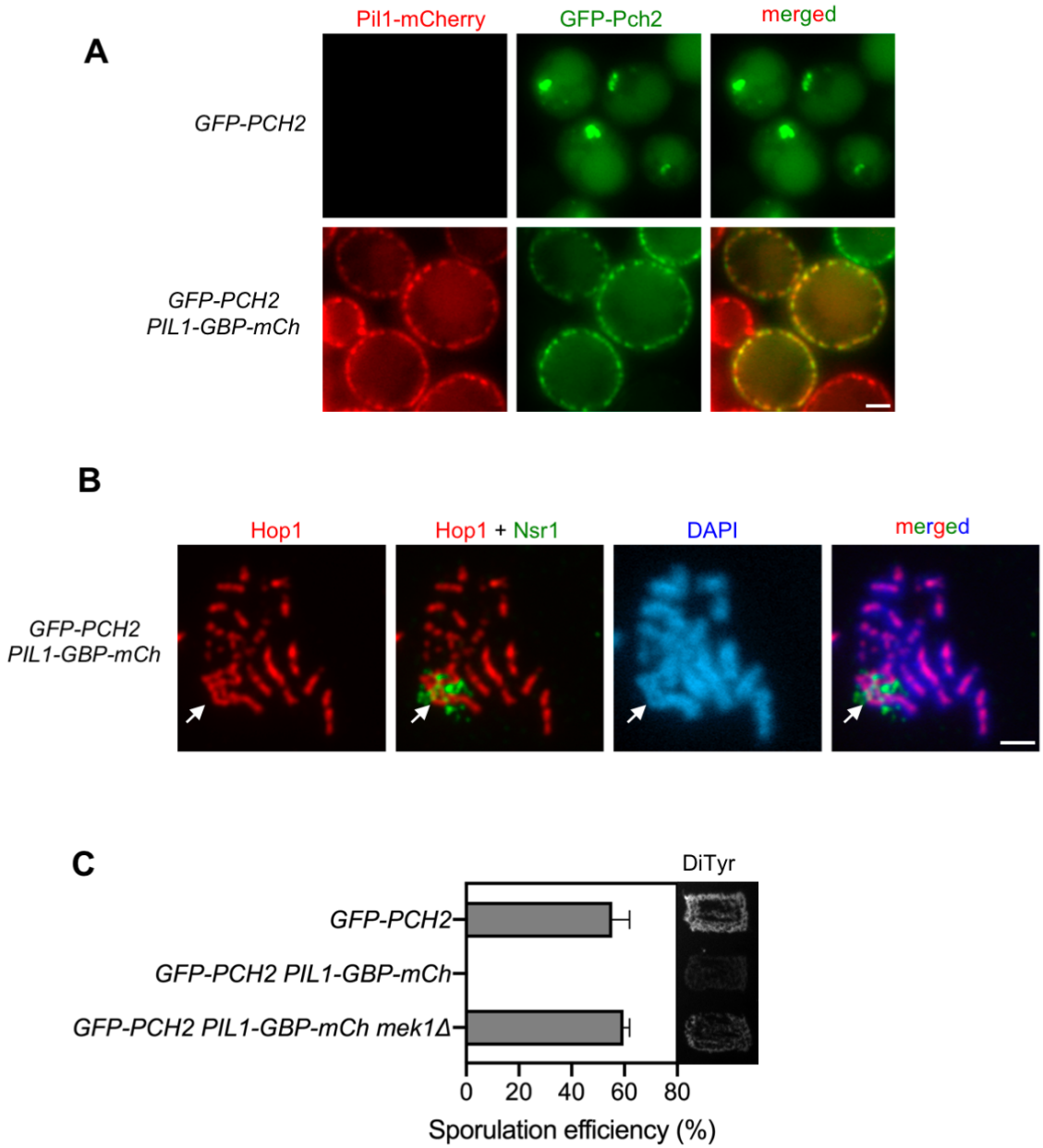

Figure S5. Pil1-GBP traps GFP-Pch2 at the plasma membrane triggering Mek1-dependent sporulation arrest.

(A) Fluorescence microscopy analysis of GFP-Pch2 and Pil1-GBP-mCherry distribution in whole meiotic cells of the indicated genotypes 16 hours after meiotic induction. Scale bar, 2 µm. **(B)** Immunofluorescence of meiotic chromosomes stained with anti-Hop1 (red) and anti-Nsr1 (nucleolar marker; green) antibodies, and DAPI (blue). The arrow points to the rDNA region. Spreads were prepared at 16 h. Scale bar, 2 µm. **(C)** Sporulation efficiency and dityrosine fluorescence (DiTyr), were examined after 3 days on sporulation plates. Error bars, SD; n=3. At least 300 cells were counted for each strain. Strains in (A-C) are: DP1624 (*GFP-PCH2*), DP1797 (*GFP-PCH2 PIL1-GBP-mCherry*) and DP1813 (*GFP-PCH2 PIL1-GBP-mCherry mek1Δ*).

Figure S6

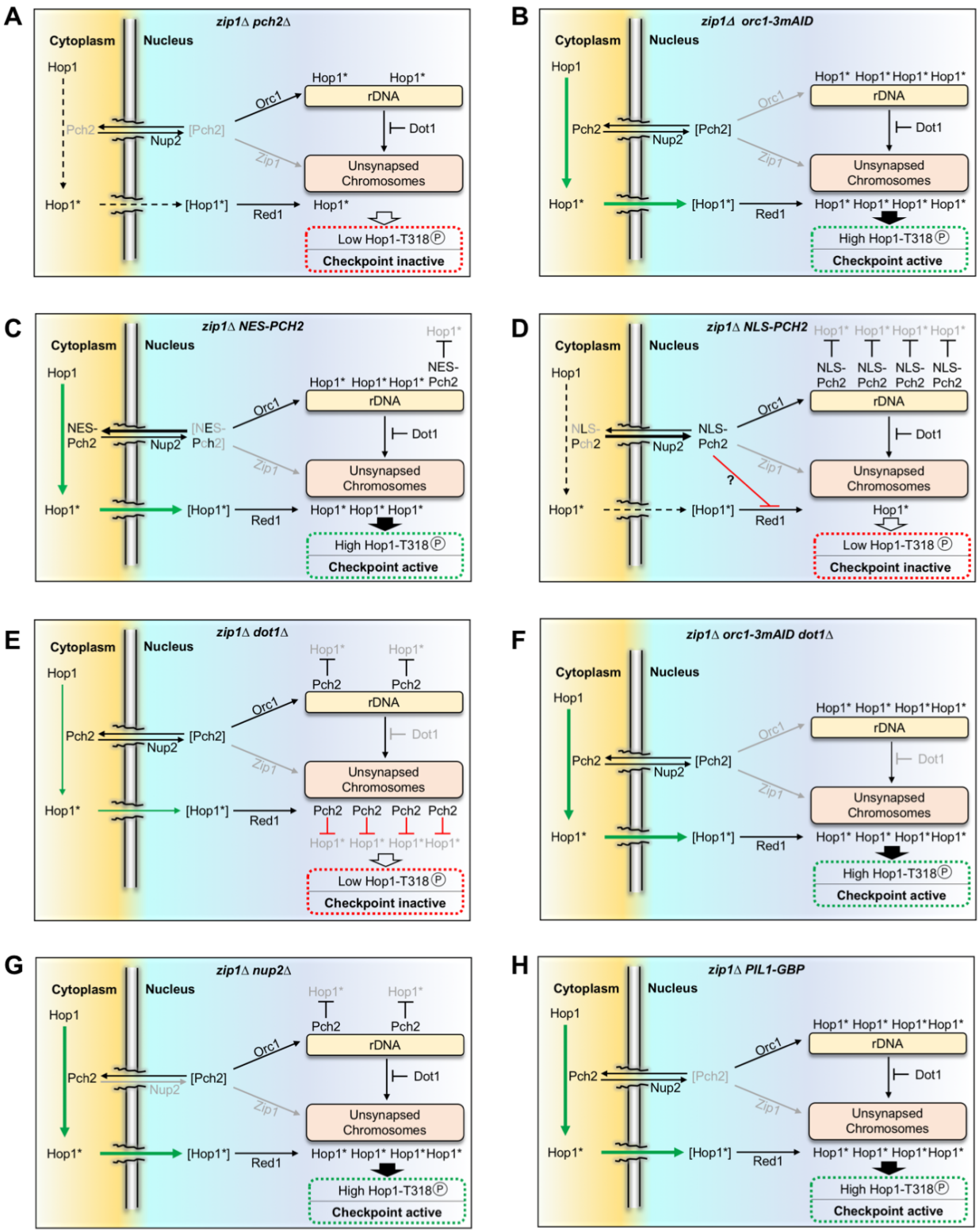
A
zip1Δ pch2Δ
Cytoplasm
Nucleus
Hop1
Pch2
[Pch2]
Nup2
Orc1
Hop1*
Hop1*
rDNA
Dot1
Zip1
Unsynapsed Chromosomes
Hop1*
[Hop1*]
Red1
Hop1*
Low Hop1-T318Ⓟ
Checkpoint inactive
B
zip1Δ orc1-3mAID
Cytoplasm
Nucleus
Hop1
Pch2
[Pch2]
Nup2
Orc1
Hop1* Hop1* Hop1* Hop1*
rDNA
Dot1
Zip1
Unsynapsed Chromosomes
Hop1*
[Hop1*]
Red1
Hop1* Hop1* Hop1* Hop1*
High Hop1-T318Ⓟ
Checkpoint active
C
zip1Δ NES-PCH2
Cytoplasm
Nucleus
Hop1
NES-Pch2
[NES-Pch2]
Nup2
Orc1
Hop1*
NES-Pch2
Hop1* Hop1* Hop1*
rDNA
Dot1
Zip1
Unsynapsed Chromosomes
Hop1*
[Hop1*]
Red1
Hop1* Hop1* Hop1*
High Hop1-T318Ⓟ
Checkpoint active
D
zip1Δ NLS-PCH2
Cytoplasm
Nucleus
Hop1
NLS-Pch2
NLS-Pch2
Nup2
Orc1
Hop1* Hop1* Hop1* Hop1*
NLS-Pch2 NLS-Pch2 NLS-Pch2 NLS-Pch2
rDNA
Dot1
Zip1
?
Unsynapsed Chromosomes
Hop1*
[Hop1*]
Red1
Hop1*
Low Hop1-T318Ⓟ
Checkpoint inactive
E
zip1Δ dot1Δ
Cytoplasm
Nucleus
Hop1
Pch2
[Pch2]
Nup2
Orc1
Hop1* Hop1*
Pch2 Pch2
rDNA
Dot1
Zip1
Unsynapsed Chromosomes
Hop1*
[Hop1*]
Red1
Pch2 Pch2 Pch2 Pch2
Hop1* Hop1* Hop1* Hop1*
Low Hop1-T318Ⓟ
Checkpoint inactive
F
zip1Δ orc1-3mAID dot1Δ
Cytoplasm
Nucleus
Hop1
Pch2
[Pch2]
Nup2
Orc1
Hop1* Hop1* Hop1* Hop1*
rDNA
Dot1
Zip1
Unsynapsed Chromosomes
Hop1*
[Hop1*]
Red1
Hop1* Hop1* Hop1* Hop1*
High Hop1-T318Ⓟ
Checkpoint active
G
zip1Δ nup2Δ
Cytoplasm
Nucleus
Hop1
Pch2
[Pch2]
Nup2
Orc1
Hop1* Hop1*
Pch2 Pch2
rDNA
Dot1
Zip1
Unsynapsed Chromosomes
Hop1*
[Hop1*]
Red1
Hop1* Hop1* Hop1* Hop1*
High Hop1-T318Ⓟ
Checkpoint active
H
zip1Δ PIL1-GBP
Cytoplasm
Nucleus
Hop1
Pch2
[Pch2]
Nup2
Orc1
Hop1* Hop1* Hop1* Hop1*
rDNA
Dot1
Zip1
Unsynapsed Chromosomes
Hop1*
[Hop1*]
Red1
Hop1* Hop1* Hop1* Hop1*
High Hop1-T318Ⓟ
Checkpoint active

Figure S6. Model of Pch2 action in different mutant conditions.

(A) In *zip1Δ pch2Δ*, the conformational change required for Hop1 chromosomal incorporation is inefficient leading to low levels of Hop1-T318 phosphorylation and checkpoint defects. **(B)** In *zip1Δ orc1-3mAID*, Pch2 is not recruited to the rDNA resulting in its accumulation in the cytoplasm fostering proficient Hop1 loading and activation. **(C)** In *zip1Δ NES-PCH2,* the balance of Pch2 distribution is biased to the cytoplasm also supporting checkpoint activation. **(D)** In *zip1Δ NLS-PCH2*, the balance of Pch2 distribution is skewed towards the nucleus resulting in the accumulation of the protein in the rDNA and the nucleoplasm. The checkpoint defect in *zip1Δ NLS-PCH2* likely stems from the reduced levels of cytoplasmic Pch2. However, since increased dosage of NLS-Pch2 causes a stronger checkpoint defect, it is possible that the accumulation of NLS-Pch2 in the nucleoplasm also exerts an inhibitory effect on checkpoint activity. **(E)** In *zip1Δ dot1Δ*, Pch2 loses its rDNA confinement and it is widely distributed throughout unsynapsed chromosomes provoking Hop1 release and, therefore, low levels of Hop1-T318 phosphorylation. **(F)** In *zip1Δ orc1-3mAID dot1Δ*, the inability of Pch2 to be recruited to the rDNA results in its exclusive cytoplasmic localization supporting checkpoint activation. Since in the absence of Orc1 there is no Pch2 to be confined in the rDNA, Dot1 is irrelevant in this context. **(G)** In *zip1Δ nup2Δ*, the pool of cytoplasmic Pch2 is increased likely reflecting a defect in Pch2 import to the nucleus in the absence of the nucleoporin; consequently, the amount of nucleolar Pch2 is reduced. The presence of Pch2 in the cytoplasm ensures an efficient checkpoint response. **(H)** In *zip1Δ PIL1-GBP*, the GFP-tagged Pch2 is sequestered in the eisosomes facing the cytoplasmic side of the plasma membrane and, therefore, being proficient in the generation of the Hop1 conformational state that facilitates chromosome incorporation. Furthermore, since in this situation Pch2 is tightly trapped outside the nucleus, any transient inhibitory effect of nuclear Pch2 is absent resulting in checkpoint hyperactivation.

Table S1. *Saccharomyces cerevisiae* strains

Strain	Genotype*	Source
BR1919-2N	*MAT*a/*MAT*α *leu2-3,112 his4-260 thr1-4 trp1-289 ura3-1 ade2-1*	Roeder Lab
DP421	BR1919-2N *lys2ΔNheI*	PSS Lab
DP422	DP421 *zip1::LYS2*	PSS Lab
DP424	DP421 *ndt80::LEU2*	PSS Lab
DP428	DP421 *zip1::LYS2 ndt80::LEU2*	PSS Lab
DP881	DP421 *zip1::LYS2 pch2::TRP1 ndt80::LEU2*	PSS Lab
DP1023	DP421 *pch2Δ::TRP1*	PSS Lab
DP1029	DP421 *zip1Δ::LYS2 pch2Δ::TRP1*	PSS Lab
DP1058	DP421 *pch2::TRP1 ndt80::LEU2*	PSS Lab
DP1151	BR1919-2N *3HA-PCH2*	PSS Lab
DP1152	BR1919-2N *zip1::LEU2 3HA-PCH2*	PSS Lab
DP1161	BR1919-2N *zip1::LEU2 pch2::TRP1*	PSS Lab
DP1164	BR1919-2N *pch2::TRP1*	PSS Lab
DP1405	DP421 *zip1::LEU2 pch2::URA3*	PSS Lab
DP1500	DP421 *zip1::LYS2 HOP1-mCherry::natMX4/HOP1*	This work
DP1620	BR1919-2N P_{HOP1}*-GFP-PCH2*	This work
DP1621	BR1919-2N *zip1::LEU2* P_{HOP1}*-GFP-PCH2*	This work
DP1624	BR1919-2N P_{HOP1}*-GFP-PCH2/pch2::TRP1*	This work
DP1625	BR1919-2N *zip1::LEU2* P_{HOP1}*-GFP-PCH2/pch2::TRP1*	This work
DP1630	BR1919-2N *zip1::LEU2* P_{HOP1}*-GFP-PCH2 orc1-3mAID::hphNT* P_{HOP1}*-OsTIR1::URA3 ndt80::kanMX3*	This work
DP1633	BR1919-2N *zip1::LEU2* P_{HOP1}*-GFP-PCH2 orc1-3mAID::hphNT* P_{HOP1}*-OsTIR1::URA3 HOP1-mCherry::natMX4/HOP1*	This work
DP1636	BR1919-2N *zip1::LEU2* P_{HOP1}*-GFP-PCH2 HOP1-mCherry::natMX4/HOP1*	This work
DP1640	BR1919-2N *zip1::LEU2* P_{HOP1}*-GFP-PCH2 ndt80::kanMX3 lys2/LYS2*	This work
DP1644	BR1919-2N *zip1::LEU2* P_{HOP1}*-GFP-PCH2/pch2::TRP1 orc1-3mAID::hphNT* P_{HOP1}*-OsTIR1::URA3*	This work
DP1650	BR1919-2N P_{HOP1}*-GFP-PCH2/pch2::TRP1 HOP1-mCherry::natMX4/HOP1 LYS2/lys2*	This work
DP1651	BR1919-2N *zip1::LEU2* P_{HOP1}*-GFP-PCH2/pch2::TRP1 HOP1-mCherry::natMX4/HOP1*	This work

DP1654	BR1919-2N *P_{HOP1}-GFP-PCH2/pch2::TRP1 ndt80::kanMX3*	This work
DP1655	BR1919-2N *zip1::LEU2 P_{HOP1}-GFP-PCH2/pch2::TRP1 ndt80::kanMX3 lys2/LYS2*	This work
DP1669	DP421 *P_{HOP1}-GFP-NES-PCH2*	This work
DP1670	DP421 *zip1::LYS2 P_{HOP1}-GFP-NES-PCH2*	This work
DP1685	DP421 *P_{HOP1}-GFP-NES-PCH2/pch2::TRP1*	This work
DP1686	DP421 *zip1::LYS2 P_{HOP1}-GFP-NES-PCH2/pch2::TRP1*	This work
DP1687	DP421 *P_{HOP1}-GFP-NES-PCH2/pch2::TRP1 HOP1-mCherry::natMX4/HOP1*	This work
DP1688	DP421 *zip1::LYS2 P_{HOP1}-GFP-NES-PCH2/pch2::TRP1 HOP1-mCherry::natMX4/HOP1*	This work
DP1695	DP421 *P_{HOP1}-GFP-NLS-PCH2*	This work
DP1696	DP421 *zip1::LYS2 P_{HOP1}-GFP-NLS-PCH2*	This work
DP1697	DP421 *P_{HOP1}-GFP-NLS-PCH2 HOP1-mCherry::natMX4/HOP1*	This work
DP1698	DP421 *zip1::LYS2 P_{HOP1}-GFP-NLS-PCH2 HOP1-mCherry::natMX4/HOP1*	This work
DP1699	DP421 *P_{HOP1}-GFP-NLS-PCH2/pch2::TRP1*	This work
DP1700	DP421 *P_{HOP1}-GFP-NLS-PCH2/pch2::TRP1 HOP1-mCherry::natMX4/HOP1*	This work
DP1701	DP421 *zip1::LYS2 P_{HOP1}-GFP-NLS-PCH2/pch2::TRP1*	This work
DP1702	DP421 *zip1::LYS2 P_{HOP1}-GFP-NLS-PCH2/pch2::TRP1 HOP1-mCherry::natMX4/HOP1*	This work
DP1723	BR1919-2N *3HA-PCH2 nup2::hphMX4*	This work
DP1724	BR1919-2N *zip1::LEU2 3HA-PCH2 nup2::hphMX4*	This work
DP1725	DP421 *P_{HOP1}-GFP-NES-PCH2/pch2::TRP1 ndt80::kanMX6*	This work
DP1726	DP421 *zip1::LYS2 P_{HOP1}-GFP-NES-PCH2/pch2::TRP1 ndt80::kanMX6*	This work
DP1729	DP421 *P_{HOP1}-GFP-NLS-PCH2/pch2::TRP1 ndt80::kanMX6*	This work
DP1730	DP421 *zip1::LYS2 P_{HOP1}-GFP-NLS-PCH2/pch2::TRP1 ndt80::kanMX6*	This work
DP1734	DP421 *zip1::LYS2 P_{HOP1}-GFP-PCH2/pch2::TRP1 dot1::URA3*	This work
DP1744	BR1919-2N *P_{HOP1}-GFP-PCH2/pch2::TRP1 nup2::hphMX4*	This work
DP1745	BR1919-2N *zip1::LEU2 P_{HOP1}-GFP-PCH2/pch2::TRP1 nup2::hphMX4*	This work
DP1746	BR1919-2N *zip1::LEU2 P_{HOP1}-GFP-PCH2/pch2::TRP1 orc1-3mAID::hphNT P_{HOP1}-OsTIR1::URA3 dot1::kanMX6*	This work
DP1747	DP421 *zip1::LYS2 P_{HOP1}-GFP-NES-PCH2/pch2::TRP1 dot1::kanMX6*	This work
DP1768	DP421 *P_{HOP1}-GFP-NLS-PCH2 ndt80::kanMX6*	This work

DP1769	DP421 *zip1::LYS2* P_{HOP1}*-GFP-NLS-PCH2 ndt80::kanMX6*	This work
DP1787	DP421 *spo11-3HA-6His::kanMX4 pch2::TRP1*	This work
DP1789	DP421 *spo11-3HA-6His::kanMX4* P_{HOP1}*-GFP-PCH2/pch2::TRP1*	This work
DP1791	DP421 *spo11-3HA-6His::kanMX4* P_{HOP1}*-GFP-NES-PCH2/pch2::TRP1*	This work
DP1792	DP421 *spo11-3HA-6His::kanMX4* P_{HOP1}*-GFP-NLS-PCH2*	This work
DP1793	DP421 *spo11-3HA-6His::kanMX4* P_{HOP1}*-GFP-NLS-PCH2/pch2::TRP1*	This work
DP1795	DP421 *PIL1-GBP-mCherry::hphMX6* P_{HOP1}*-GFP-NES-PCH2/pch2::TRP1*	This work
DP1796	DP421 *zip1::LYS2 PIL1-GBP-mCherry::hphMX6* P_{HOP1}*-GFP-NES-PCH2/pch2::TRP1*	This work
DP1797	BR1919-2N *PIL1-GBP-mCherry::hphMX6* P_{HOP1}*-GFP-PCH2/pch2::TRP1 LYS2/lys2*	This work
DP1802	DP421 *PIL1-GBP-mCherry::hphMX6 3HA-PCH2*	This work
DP1803	DP421 *zip1::LEU2 PIL1-GBP-mCherry::hphMX6 3HA-PCH2*	This work
DP1811	DP421 *PIL1-GBP-mCherry::hphMX6* P_{HOP1}*-GFP-NES-PCH2/pch2::TRP1 mek1::natMX4*	This work
DP1812	DP421 *zip1::LYS2 PIL1-GBP-mCherry::hphMX6* P_{HOP1}*-GFP-NES-PCH2/pch2::TRP1 mek1::natMX4*	This work
DP1813	BR1919-2N *PIL1-GBP-mCherry::hphMX6* P_{HOP1}*-GFP-PCH2/pch2::TRP1 mek1::natMX4 LYS2/lys2*	This work

*All strains are diploids isogenic to BR1919 and, unless specified, homozygous for the indicated markers. DP421 is a *lys2* version of the original BR1919-2N.

Table S2. Plasmids

Plasmid name	Vector	Relevant parts	Source/Reference
pSS383	pFA6a	*GBP-mCherry::hphMX6*	A. Fernández-Álvarez
pSS393	pRS314	*TRIP1 CEN6* P_{HOP1}*-GFP-PCH2*	(Herruzo et al., 2019)
pSS408	pRS314	*TRIP1 CEN6* P_{HOP1}*-GFP-NES-PCH2*	This work
pSS421	pRS314	*TRIP1 CEN6* P_{HOP1}*-GFP-NLS-PCH2*	This work
pSK54	pRS306	*URA3 spo11-3HA-6His::kanMX4*	(Kee and Keeney, 2002)

Table S3. Primary antibodies

Antibody	Host and type	Application* (Dilution)	Source / Reference
Hop1 (5C12E8)	Mouse monoclonal	WB (1:2000)	(Herruzo et al., 2019)
Hop1	Rabbit polyclonal	IF (1:300)	(Smith and Roeder, 1997)
Hop1-T318-ph	Rabbit polyclonal	WB (1:1000)	(Penedos et al., 2015)
H3-T11-ph	Rabbit polyclonal	WB (1:2000)	Abcam ab5168
Pgk1 (22C5D8)	Mouse monoclonal	WB (1:5000)	Molecular Probes 459250
Pch2	Rabbit polyclonal	WB (1:2000)	(Herruzo et al., 2019)
Nsr1 (31C4)	Mouse monoclonal	IF (1:200)	ThermoFisher MA1-10030
mAID (1E4)	Mouse monoclonal	WB (1:400)	MBL M214-3
GFP (JL-8)	Mouse monoclonal	IF (1:200)	Clontech 632381

*WB, western blot; IF, immunofluorescence

Supplemental References

Herruzo, E., B. Santos, R. Freire, J.A. Carballo, and P.A. San-Segundo. 2019. Characterization of Pch2 localization determinants reveals a nucleolar-independent role in the meiotic recombination checkpoint. *Chromosoma*. 128:297-316.

Kee, K., and S. Keeney. 2002. Functional interactions between *SPO11* and *REC102* during initiation of meiotic recombination in *Saccharomyces cerevisiae*. *Genetics*. 160:111-122.

Penedos, A., A.L. Johnson, E. Strong, A.S. Goldman, J.A. Carballo, and R.S. Cha. 2015. Essential and Checkpoint Functions of Budding Yeast ATM and ATR during Meiotic Prophase Are Facilitated by Differential Phosphorylation of a Meiotic Adaptor Protein, Hop1. *PLoS One*. 10:e0134297.

Smith, A.V., and G.S. Roeder. 1997. The yeast Red1 protein localizes to the cores of meiotic chromosomes. *J Cell Biol*. 136:957-967.